DISASTER PREVENTION RESEARCH INSTITUTE

BULLETIN No. 9 APRIL, 1955

EXPERIMENTAL STUDIES ON METEOROLOGICAL TSUNAMIS TRAVELING UP THE RIVERS AND CANALS IN OSAKA CITY

BY

SHOITIRO HAYAMI, KATSUMASA YANO,
SHOHEI ADACHI AND HIDEAKI KUNISHI

KYOTO UNIVERSITY, KYOTO, JAPAN

DISASTER PREVENTION RESEARCH INSTITUTE
KYOTO UNIVERSTY

BULLETINS

Bulletion No. 9 April, 1955

Experimental Studies on Meteorological Tsunamis Traveling up the Rivers and Canals in Osaka City

By

Shoitiro HAYAMI, Katsumasa YANO,
Shohei ADACHI and Hideaki KUNISHI

Contents

1. General Description

1.1. Object of Experiment

The objects of this experiment were to clarify the changes in height of meteorological tidal waves (Tsunamis) traveling up the estuaries of rivers and canals in Osaka City and to determine a reasonably designed elevation for the prevention embankments along the estuaries for the meteorological bore in Osaka Bay, Japan. In Japan, typhoons attack the land almost every year as shown in Fig. 1 and cause tremendous disasters due to flood innundations, tsunamis, land slides, etc.. The "Jane-typhoon" which attacked the Osaka district, a commercial center of Japan, on September 3, 1950, caused one of the severest disasters. The area innundated by meteorologi-

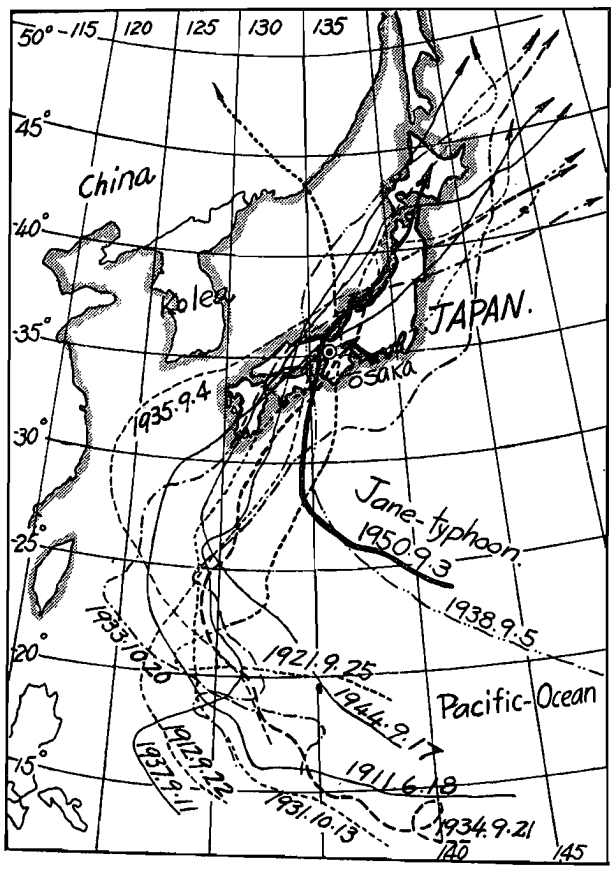

Fig. 1. Tracks of main typhoons.

cal tidal bore was 56.25 km², about one-third of the whole area of Osaka City, and the damage was estimated to be about 200 billion "Yen" (550 million dollars).

Immediately after the disaster, the government office of Osaka Prefecture planned a rehabilitation program according to which the commercial, industrial and residental districts were wholly to be surrounded by embankment levees (total length 80.0 km, top elevation O. P. +7.00 ~ 4.00 m*), gates and locks, as shown in Fig. 2.

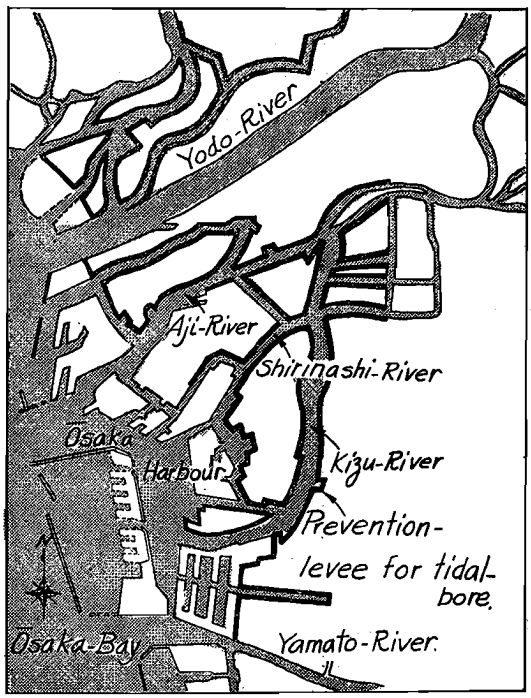

Fig. 2. Designed levee net of Osaka City.

In October, 1950, the rehabilitation work was begun and continued up to the end of 1954, when the greater part of the work had been completed. At the first stage of planning the embankment, many of the engineers and scientists discussed the problem as to whether the height of tidal bores would be augmented or reduced in narrow channels by friction factors or some other causes. To clarify these points, the authors made model experiments

* O.P. means the Osaka Bay Datum Level, indicating approximately the lowest low water in the Bay.

by the following plan and method.

1.2. Course of Experimental Research

This experimental research was carried out under contract with Osaka Prefecture. After designs of model plants and measuring instruments were finished, the authors started to build the models on August, 1952 at the Hydraulic Laboratory of their Institute, and at the same time began to investigate fundamental problems relating to the hydraulic similitude and the possibility of generating artificial bores by an in-door small scale channel in the laboratory.

At the beginning the artificial generation of bores was one of the most important and the most difficult problems. The authors ascertained the reliability of the pneumatic wave generator and decided to adopt it.

In addition to this, the authors tried to clarify theoretically and experimentally the relations of hydraulic similitudes, especially those of roughness, considering the distortion effected by the models. About one year was devoted to these preliminary investigations, after which the experiment proper was started in March, 1954, and completed in April, 1954.

2. Experimental Plant

2.1. Model Itself

The scale of the model was selected to be 1 : 500 horizontally and 1 : 50 vertically. The model was 20.0 m wide and 40.0 m long, as shown in Photo. 1, which is assumed to represent the actual area, 10 km north to south, and 20 km east to west, containing, Yodo River, Aji River, Shirinashi River, Kizu River, and many other small rivers and canals in Osaka City.

The rivers and canals in the model were built of bricks and their surfaces

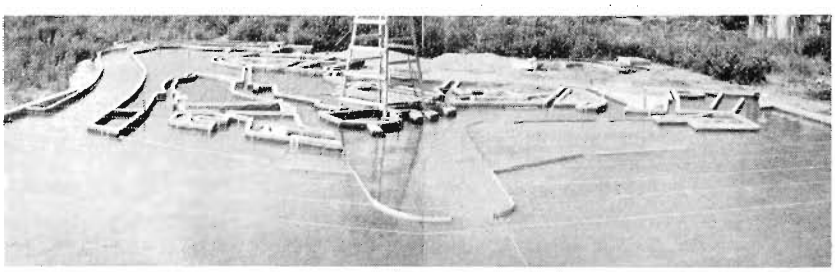

Photo. 1. General view of the model.

were finished with 1 : 3 mortar. Small wooden segments were attached to the channels so as to simulate the actual roughness as shown in Photo. 2.

2.2. Wave Generator

Photo. 2. Model channel with artificial roughness.

To generate artificially the meteorological bore, associated with the "Jane typhoon" of September, 1950, the pneumatic type of wave generator, as shown in Photo. 3, was adopted.

The location of the generator in the model was so chosen as to lie along the 10.0 m depth contour under the mean sea level of Osaka Bay.

The wave generator consisted of an air chamber which absorbed the water mass by withdrawing the inner air through a blower.

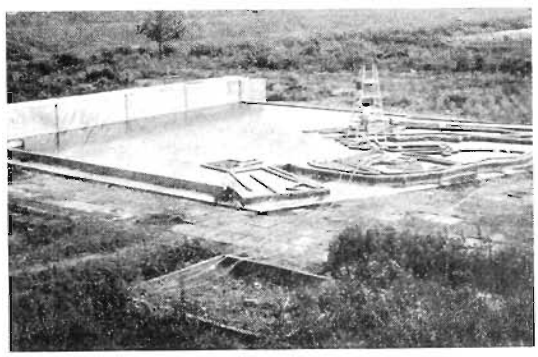

Photo. 3. Pneumatic wave generator.

It ejected out the water by forcing the air through an air intrusion chamber. The air intrusion chamber could regulate the pressure in the air chamber so as to simulate the desired type of meteorological bore. The air chamber was a hollow box of reinforced concrete with a slit of 0.3m in width through which the bore was flushed out into the model bay. The main dimensions of the air chamber are shown in Fig. 3.

Outside the air chamber, a 5-HP. Routs-Blower was set, and outside the air intrusion chamber, 25 valves with seven different diameters varying from 1/4" to 4" were arranged. By regulating these 25 valves, an arbitrary bore could be generated. In the present experiment the authors produced the desired type of meteorological bore by hand manipulation, though they intend

to adopt an electric automatic control system in near future.

In the following, the action of the wave generator will be given, where

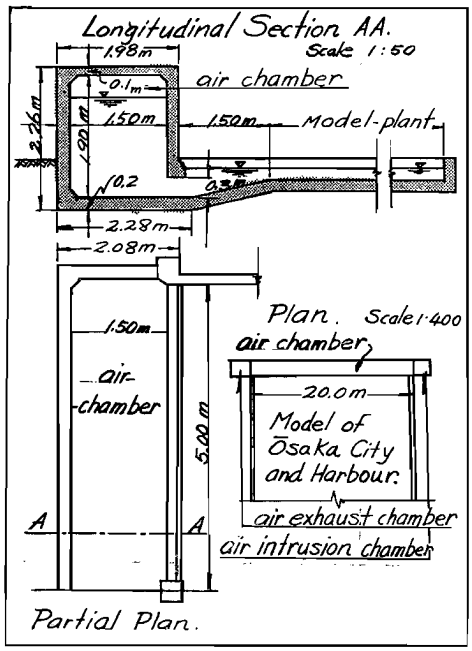

Fig. 3. Pneumatic wave generator.

P_a = atmospheric pressure,

P = air pressure in the air chamber,

ρ_a = density of air at normal condition,

ρ = density of air in the air chamber,

ρ_w = density of water,

U_a = intrusion velocity of air into the air chamber,

C_a = coefficient of intrusion at the intrusion hole,

U_w = flushing out velocity of water through the opening of the air chamber,

C_w = coefficient of flushing out through opening,

S_1 = cross sectional area of the intrusion hole,

S_2 = horizontal area of the air chamber

S_3 = vertical cross sectional area of the opening,

S_4 = horizontal area of mobel bay,

η = vertical water level difference between the air chamber and area outside model,

η^* = depth of air layer in the air chamber

η_0^* = initial depth of air layer in the air chamber,

η_0 = initial water level difference,

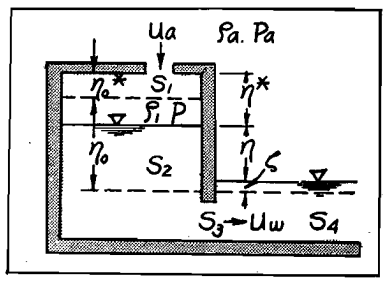

Fig. 4. Notations for the analysis of air chamber.

ζ = wave height, generated in model bay.

Then the equations of motion and continuity would be

$$U_a=\sqrt{2g\,(P_a-P)\,\frac{\rho_w}{\rho_a}} \quad \cdots\cdots(2.1),$$

$$C_a\cdot\rho_a\cdot U_a\cdot S_1=\frac{d}{dt}\,(\rho\cdot\eta^*\cdot S_2) \quad \cdots\cdots(2.2).$$

Since air intrusion is effected gradually, the change may be considered to be isothermal,

namely

$$\frac{P}{\rho} = \frac{P_a}{\rho_a} = \text{constant.}$$

From equations (2.1) and (2.2),

$$S_1 = \frac{S_2}{C_a\cdot P_a\sqrt{2g(P_a-P)\frac{\rho_w}{\rho_a}}}\ \frac{d}{dt}(P\cdot\eta^*) \quad \cdots\cdots(2.3).$$

Next, the equations of motion and continuity at the flushing out point of the water will be given by

$$U_w=\sqrt{2g\{\eta-(P_a-P)\}} \quad \cdots\cdots(2.4),$$

$$C_w\cdot U_w\cdot S_3=S_2\,\frac{d\eta^*}{dt}=-S_2\frac{d}{dt}\,(\eta+\zeta) \quad \cdots\cdots(2.5).$$

Assuming that the water level of the model bay increases uniformly in vertical as well as horizontal directions,

$$C_w\cdot U_w\cdot S_3=S_4\frac{d\zeta}{dt} \quad \cdots\cdots(2.6).$$

By equations (2.4), (2.5) and (2.6), the following relationships would be established,

$$\frac{d\eta^*}{dt}=\frac{S_4}{S_2}\cdot\frac{d\zeta}{dt} \quad \cdots\cdots(2.7),$$

$$\frac{dP}{dt}=\frac{d\zeta}{dt}\left\{1+\frac{S_4}{S_2}+\frac{1}{g}\left(\frac{S_4}{C_w\cdot S_3}\right)^2\frac{d^2\zeta}{dt^2}\right\} \quad \cdots\cdots(2.8).$$

Integrating these equations,

$$\eta^* = \eta_0^* + \frac{S_4}{S_2} \cdot \zeta \quad \cdots\cdots (2.9),$$

$$P = (P_0 - \eta_0) + \frac{1}{2g}\left(\frac{S_4}{C_w \cdot S_3}\right)^2 \left(\frac{d\zeta}{dt}\right)^2 + \zeta\left(1 + \frac{S_4}{S_2}\right) \quad \cdots\cdots (2.10).$$

Substituting equations (2.9) and (2.10) into equation (2.3), the relation between S_1 and ζ may be obtained.

2.3. Artificial Roughness of Model Channels

In order that the model flow be dynamically similar to the actual flow, the ratio of each of the corresponding terms in both equations of motion and continuity must be equal.

In the present case, the fundamental equations of the following types are given:

$$\frac{\partial U}{\partial t} + U\frac{\partial U}{\partial x} = -\frac{\lambda}{2R}U^2 + g\left(i - \frac{\partial h}{\partial x}\right) \quad \cdots\cdots (2.11),$$

$$\frac{\partial A}{\partial t} + \frac{\partial}{\partial x}(A \cdot U) = 0 \quad \cdots\cdots (2.12),$$

where U = mean velocity in x-direction,
h = water depth,
R = hydraulic mean depth,
i = channel bed slope,
λ = friction coefficient,
g = gravity acceleration,
A = cross sectional area.

Denoting the suffix 1 for actual flow and 2 for model flow, and equalizing the ratio of each of the corresponding terms in equations (2.11) and (2.12),

$$\frac{U_2}{U_1} \cdot \frac{t_1}{t_2} = \left(\frac{U_2}{U_1}\right)^2 \frac{x_1}{x_2} = \frac{\lambda_2}{\lambda_1} \cdot \frac{R_1}{R_2}\left(\frac{U_2}{U_1}\right)^2 = \frac{h_2}{h_1} \cdot \frac{x_1}{x_2} \quad \cdots (2.13),$$

$$\frac{A_2}{A_1} \cdot \frac{t_1}{t_2} = \frac{U_2}{U_1} \cdot \frac{A_2}{A_1} \cdot \frac{x_1}{x_2} \quad \cdots\cdots (2.14).$$

From these equations, the following relations will be derived.

$$\frac{\lambda_2}{\lambda_1} = \frac{R_2}{R_1} \cdot \frac{x_1}{x_2} \quad \cdots\cdots (2.15),$$

$$\frac{t_2}{t_1}=\frac{x_2}{x_1}\cdot\left(\frac{h_2}{h_1}\right)^{-\frac{1}{2}} \quad \cdots\cdots\cdots\cdots\cdots\cdots(2.16).$$

Equation (2.15) gives the relation between the frictional resistances, and equation (2.16) the relation between the time scales, the latter indicating that Froude's number must be constant. The relation between roughnesses would be derived from equation (2.15).

The resistance law pertaining to the turbulent flow in the rough channel bed is given by the following,

$$\sqrt{\frac{2}{\lambda}}=A_r+\frac{1}{x}ln\frac{R}{k}+\delta \quad \cdots\cdots\cdots\cdots\cdots (2.17)$$

where A_r = constant, depending upon roughness

x = mixing distance in turbulent flow

k = roughness height in bed

δ = correction factor for effects due to the sectional form of channel, non-uniformity of both free surface and shearing force.

Inserting equation (2.17) into equation (2.15),

$$\frac{A_{r1}+\frac{1}{x_1}ln\frac{R_1}{k_1}+\delta_1}{A_{r2}+\frac{1}{x_2}ln\frac{R_2}{k_2}+\delta_2}=\left(\frac{R_2}{R_1}\right)^{\frac{1}{2}}\left(\frac{x_1}{x_2}\right)^{\frac{1}{2}}$$

so

$$\frac{k_2}{R_2}=\left(\frac{k_1}{R_1}\right)^{\frac{x_2}{x_1}\left(\frac{R_2}{R_1}\right)^{-\frac{1}{2}}\left(\frac{x_1}{x_2}\right)^{-\frac{1}{2}}} exp\, x_2\left[\left\{A_{r2}-\left(\frac{R_2}{R_1}\right)^{-\frac{1}{2}}\left(\frac{x_1}{x_2}\right)^{-\frac{1}{2}}A_{r1}\right\}\right.$$

$$\left.+\left\{\delta_2-\left(\frac{R_2}{R_1}\right)^{-\frac{1}{2}}\left(\frac{x_1}{x_2}\right)^{-\frac{1}{2}}\delta_1\right\}\right] \cdots\cdots\cdots\cdots\cdots\cdots(2.18).$$

Assuming $x_1=x_2=x$ and $A_{r1}=A_{r2}=A_{ro}$ and also putting

$$p=\left(\frac{R_2}{R_1}\right)^{-\frac{1}{2}}\left(\frac{x_1}{x_2}\right)^{-\frac{1}{2}} \quad \cdots\cdots\cdots\cdots\cdots\cdots(2.19),$$

and

$$q=exp\ x\ \{A_{ro}(1-p)+(\delta_2-p\delta_1)\} \quad \cdots\cdots\cdots\cdots (2.20),$$

equation (2.18) will be transformed to a single form

$$\frac{k_{s2}}{R_2} = q\left(\frac{k_{s1}}{R_1}\right)^p \quad \cdots\cdots(2.21),$$

where k_s means the equivalent sand roughness.

As seen from equation (2.21), if the value of k_{s1} in the actual flow is known, then the value of k_{s2} in the model flow will be determined. The value of k_{s1} may be obtained from a coefficient of roughness such as Manning's in the channel

$$n^2 = \lambda \frac{R^{\frac{1}{3}}}{2g} \quad \cdots\cdots(2.22).$$

Substituting equation (2.22) into equation (2.17),

$$n = g^{-\frac{1}{2}} \cdot R^{\frac{1}{6}} \Big/ \left(A_{r0} + \frac{1}{\varkappa} ln \frac{R}{k_s} + \delta\right)$$

or

$$\frac{k_s}{R} = exp\, \varkappa \left(A_{r0} + \delta - g^{-\frac{1}{2}} \cdot R^{\frac{1}{6}} \cdot n^{-1}\right) \quad \cdots\cdots(2.23).$$

Since it is very hard to determine the value of n in the tidal rivers in Osaka City, the value of n is assumed to be $n = 0.03$ and the values of A_{r0}, $\varkappa$ to be $A_{r0} = 6.0$, $\varkappa = 0.4$, by the experimental data of Y.Iwagaki,[1] Assistant Professor of Kyoto University.

As to the correction factor δ, the effect due to non-uniformity of the free surface and the shearing stress is neglected, and only the effect due to the forms of the channel section is considered.

On this effect, G. H. Keulegan[2] proposed the following equation for a rectangular section.

$$\delta = \frac{B}{\varkappa} = \frac{1}{\varkappa}\left\{ln\left(1 + \frac{2h}{B}\right) - \frac{h}{B}\right\} \quad \cdots\cdots(2.24),$$

where h = water depth

B = channel width.

Fig. 5 shows the value of k_{s1} against h/B and R_1 by equation (2.23). Though the value of k_{s2}, corresponding to k_{s1}, can be computed by the equations (2.19), (2.20) and (2.21), it can be also determined easily by the graphical method.

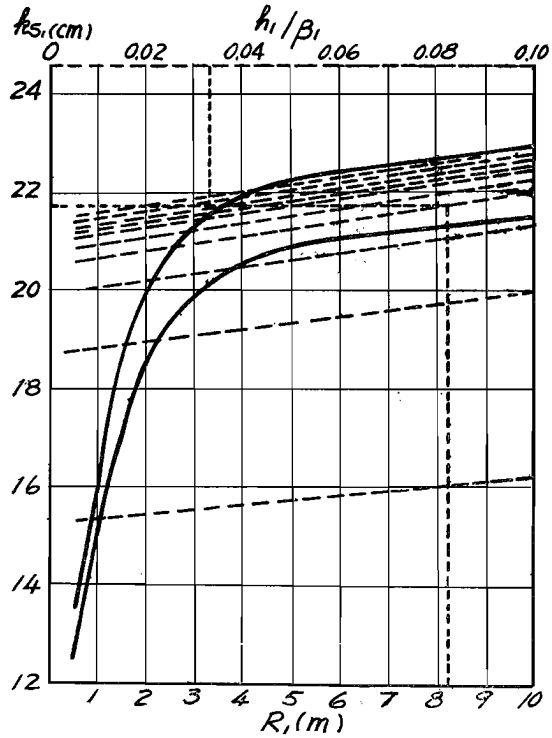

Fig. 5. Values of k_{s1} corresponding to Manning's coefficient, $n = 0.03$. Full line: equal h_2/B_2-line, upper $h_1/B_1 = 0.1$, lower $h_1/B_1 = 0.005$. Broken line : equal R_1-line, uppermost $R_1 = 10$ m, lowest $R_1 = 1$m, interval of successive line=1m.
Use of the diagram.
Given R_1 or h_1/B_1, then k_{s1} is obtained on equal R_1- or h_1/B_1-line for any value of h_1/B_1 or R_1.

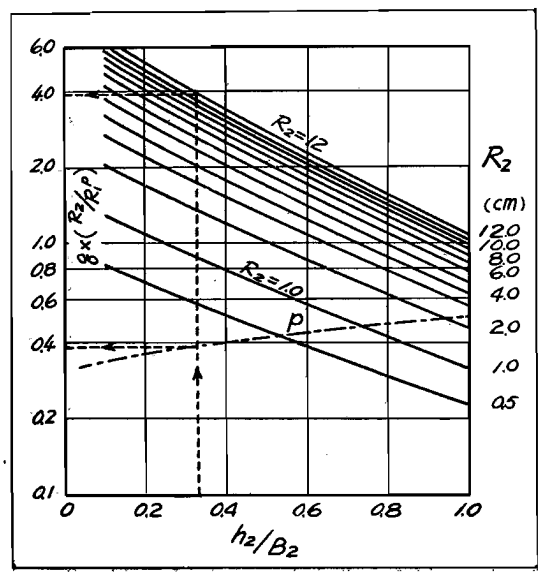

Fig. 6. Values of p and q (R_2/R_1^p) in rectangular cross section channel ($x_2/x_1 = 1/500$, $h_2/h_1 = 1/50$). Ordinate: p and $q\cdot(R_2/R_1^p)$. Full line: h_2/B_2-$q\cdot(R_2/R_1^p)$ relation for constant R_2. Broken line: h_1/B_1-p relation.
Use of the diagram.
For any given value of h_2/B_2 (i.e. R_2/R_1), p and $q\cdot(R_2/R_1^p)$ are obtained on their respective relation curves.

Fig. 6 shows the equations (2.19), (2.20) and Fig. 7 the equation (2.21).

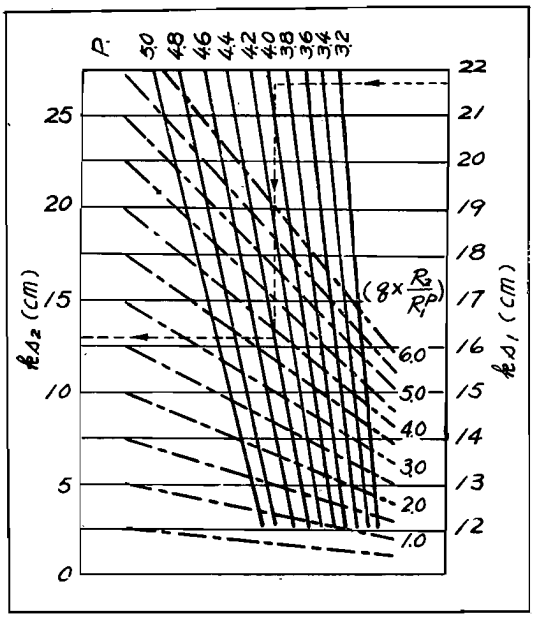

Fig. 7. k_{s1}-k_{s2} diagram. Abscissa is $(k_{s1})^p$. Full line: k_{s1}-$(k_{s1})^p$ relation for constant p (the value of p in the diagram are erroneous. They must be divided by 10). Broken line; k_{s2}-$(k_{s1})^p$ (relation for constant $q\cdot(R_2/R_1^p)$.
Use of the diagram.
Based on the values of k_{s1}, p and $q\cdot(R_2/R_1^p)$ obtained from Figs. 5 and 6, we proceed the path as indicated by the arrows, then the corresponding value of k_{s2} is obtained.

By these diagrams the value of k_{s2} in the model channel can very easily be obtained. Then, next step would be to give the model channel

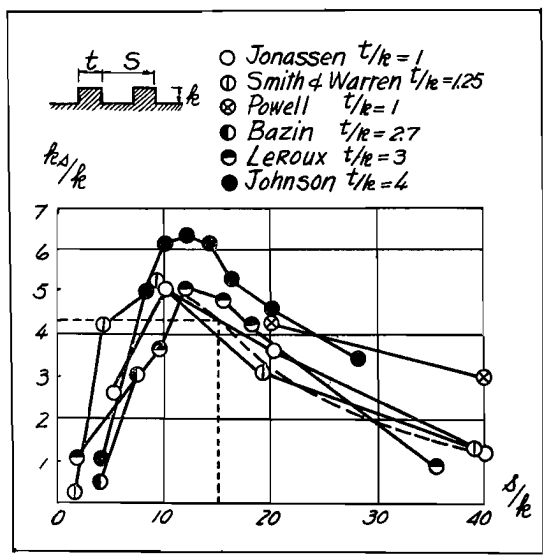

Fig. 8. $k_s/k-S/k$ diagram.

an artificial roughness equivalent to the calculated one.

By following J.W.Johnson's experiments[3] on rectangular wooden ridges normal to the direction of flow, the relations between ridge width t, pitch s, height k, and equivalent roughness were obtained. Fig. 8 of this relation shows that k_s/k becomes maximum for $s/k=10\sim12$ and $k_s/k \simeq 5$ for $t/k = 1$.

It is also recognized by Mr. Hosoi[4] and H. Schlichtung[5] that the value of k_s/k becomes maximum for $s/k=10\sim12$. By this diagram (Fig. 8), t and s were calculated and tabulated.

Basing on these calculations, wooden rectangular ridges (as shown in photo. 2) with the height of 1,0, 1.5, 2.0, 2.5 and 3.0 cm, and $t/k=1$, were set in the model channels.

3. Measuring instruments

3.1. Self-recording Wave-meter

Because of the instrumental sensitivity required for measuring the minute variations in water level, an electromagnetic wave-meter (Fig. 9) was designed and constructed after much theoretical computation and experimental research.

The sensing elements consisted of two partially submerged parallel wires or plates at a proper distance apart. Under a proper voltage between these two poles the variations in water level were obtained through those in electric current, which were recorded by an oscillograph.

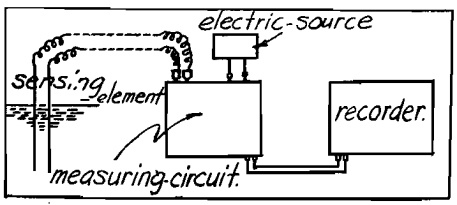

Fig. 9. Electromagnetic wave-meter

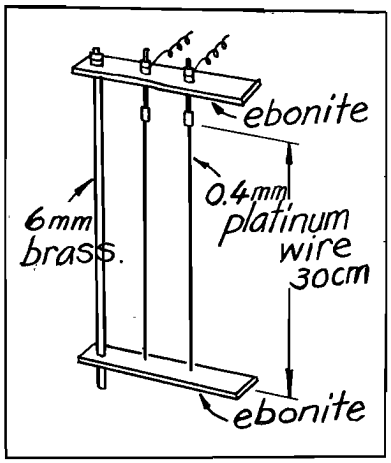

Fig. 10. Sensing element.

Two platinum wires, 0.4 mm in diameter and 30.0 cm in length, were used as the poles, as shown in Fig. 10. Instead of platinum wires, stainless steel and tungsten wires in pairs were also used successfully, but nickel galvanized copper wires were not recommended because of the measurement being unstable due to electrolysis.

The recording instrument was an electromagnetic oscillograph, as shown in photo. 4, whose galvanometers were of the moving coil type with 15 and 1 *c.p.s.* free oscillations and had the sensitivity of about 8×10^{-8} *A*.

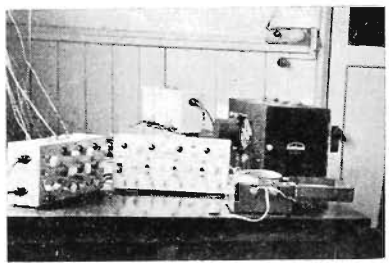

Photo. 4. Recording part of wave meter.

3.2. Measuring Circuit

For this circuit the following conditions were necessary.

(1). To avoid electrolysis, it was necessary to utilize an alternating current of at least 60 *c.p.s.*, although it should be rectified for the galvanometer.

(2). To make a linear calibration, the circuit had to possess the property of inverse proportionality of galvanometer current to sensing element resistance. Because the electric resistance x between the two poles varies in inverse proportion to the length l of the wire submerged in the water,

$$x = \alpha/l \quad \cdots\cdots (3.1)$$

where α is a proportional constant, and depends on the quality of the water, water temperature, interval between two poles, diameter of wire, and intensity of electric current. In this experiment, in which the platinum wires, 0.4 mm in diameter with 1.0 cm interval, was used at normal temperature, the value of α was about 2×10^4 *ohm*/cm.

(3). To maintain the voltage stabilization of the order of at least 0.1 *volt* for the supplied electric source of 100 *volts* because of the characteristic properties of the rectifier.

To satisfy these necessary conditions, the circuit shown in Fig. 11 was devised. More details will be explained below. The authors utilized the characteristic properties of the rectifiers at about 2.0 *volts A.C.* between both terminals of a copper dioxide rectifier for 1 *m.A.*

The rectified electric current, (the order of which was about 2×10^{-4} A under 6 $K\Omega$ load,) can be not always neglected, compared with that of the electric currents in the bridge parts, but, for convenience, the general properties of this circuit were studied theoretically, neglecting the rectified current.

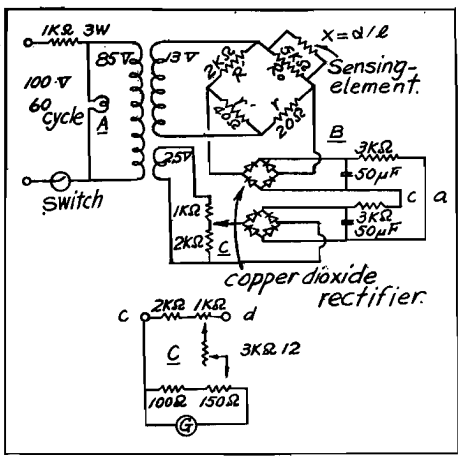

Fig. 11. Measuring circuit.

Using the notations expressed in Fig. 11, and putting

$$f = \frac{r}{R_0}, \qquad f' = \frac{r'}{R'},$$

the electric voltage between both terminals of the rectifier under the condition of

$$r \ll x = \frac{a}{l}$$

is given as follows,

$$\frac{V}{(1+f)(1+f')}\left\{(f'-f)-\frac{r}{a}\cdot l\right\}\times\left(1-\frac{\frac{r}{a}\cdot l}{1+f}\right) \quad \cdots(3.2)$$

where V is the secondary voltage of the transformer.

In this equation, if the value of $\frac{r}{a}\cdot l/(1+f)$ is made as small as possible, the variation in voltage will become proportional to that of the water

level, i.e. the value of l.

It is necessary to maintain the stationary voltage $V(f'-f)/(1+f)(1+f')$ of about 2.0 *volts* because of the characteristics of the rectifiers.

Now, this value is expressed as *a-volt*. It is also necessary to restrict the changing voltage expressed as *b-volt*, at most within the range of 0.5 *volt*, in order to obtain a linear property in calibration. Because of the bridge circuit itself, it is desirable to secure a degree of linearity $\frac{r}{a} \cdot l/(1+f)$ within the order of 1/100. This value is expressed as σ.

Namely

$$a = \frac{V(f'-f)}{(1+f)(1+f')} \quad \cdots\cdots(3.3),$$

$$b = \frac{V}{(1+f)(1+f')} \cdot \frac{r}{a} \cdot l_{max} \quad \cdots\cdots(3.4),$$

$$\sigma = \frac{\frac{r}{a} \cdot l_{max}}{1+f} \quad \cdots\cdots(3.5).$$

Solving these equations for f, f', and r yields

$$f = \frac{V - \left(a + \frac{b}{\sigma}\right)}{a + \frac{b}{\sigma}} \quad \cdots\cdots(3.6),$$

$$f' = \frac{\sigma}{b} V - 1 \quad \cdots\cdots(3.7),$$

$$r = \frac{\sigma V}{a + \frac{b}{\sigma}} \cdot \frac{a}{l_{max}} \quad \cdots\cdots(3.8).$$

Thus, the electric resistance to be set in the circuit can be expressed in terms of a, b, σ, l_{max} and V.

It must be noticed that the secondary voltage V has to have a lower limit in order to gain a higner linearity, i.e.

$$V > a + \frac{b}{\sigma} \quad \cdots\cdots(3.9).$$

In this way, the circuit was finally determined as shown in **Fig.** 11. The secondary voltage V of 13.0 *volts* was determined for the assumed value of

$\sigma = 1/50$, while the observed value of σ was 1/120, indicating a complete linearity in practice.

This was due to a slight deviation resulting from the nonlinear characteristic of the rectifier. The case of $a = 2$ *volts* and $b = 0.2$ *volts* was utilized successfully. In Fig. 11, A is the part of the voltage regulation. In this part, a neontube, which had a property of discharge under a constant voltage, has been set up on the primary side of the transformer.

B is the main part in this circuit and contained an electrolytic condenser of 50 μF for preventing fluctuation in the rectified current. C is the compensating circuit and supplies the current which cancels the prescribed stationary current from B. Therefore, it also served for the zero-point regulation of the images on the recorder, and was used as an aid in voltage regulation by connecting it on the same transformer. D is the sensitivity regulation part which can be regulated in eleven steps of magnification, from 3 times to 1/10 times. A more precise regulation of the magnification was done by a 1 $K\Omega$ variable resistor. The 150 Ω variable resistor was used mainly for regulating the non-uniformity of the sensitivities of the galvanometers. A shunt resistance of 250 Ω was selected because the resistance in the critical damping of the galvanometer with 1 *c. p. s.* was 250 Ω.

By this instrument, measurements of 0.2 mm variation in water level were made satisfactory with careful treatment.

3.3. Current-meter (velocity measurement)

To measure the current velocity, a number of small propeller type current meters of 3.0 cm in diameter were used. Their circuits are shown in Fig. 12.

Being connected to an oscillograph, the variation of current velocity was recorded electromagnetically.

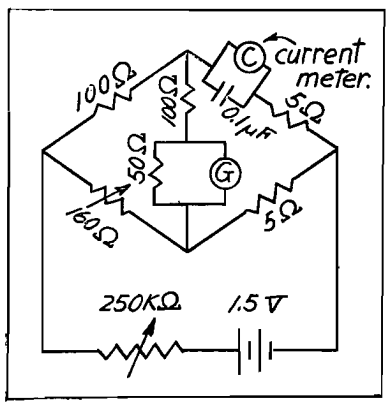

Fig. 12. Circuit of current

4. Preliminary Experiments

4.1. The First Preliminary Experiment

The object of the first preliminary experiment was to investigate the reliability of the pneumatic wave-generator and also to study the propagation of perturbation generated by it in a channel.

It is difficult to regenerate a meteorological bore, owing to its irregular form, long wave-length and wide width. The usual types of wave generators such as vibrating and plunger types were not suitable for the present asymmetrical wave from the point of structure and operation. So a pneumatic wave generator of the type used for the estuary experiment in Thames River in England[6] was abopted.

To ascertain its feasibility, a preliminary trial test was made by means of a small scale plant as shown in Fig. 13 which consisted of a small glass box of 20, 22 and 57 cm, and a wooden channel of rectangmlar section of 10, 15 cm section and 25.4 m long.

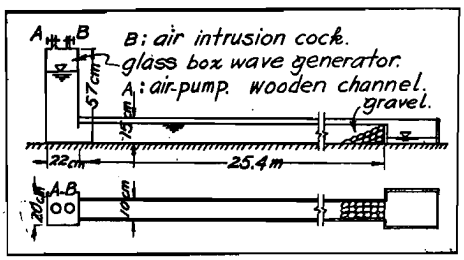

Fig. 13. Preliminary experimental channel.

The wave generator glass box had the air intrusion hole A and air exhaust hole B, and a 1/4 HP. vacuum pump was connected to A and a glass cock was set at B, both of which could regulate and generate any desired wave form. By this small scale plant, the possibility and the reliability of this type of wave generator were ascertained. Then the propagation of solitary waves generated by it were observed in the channel. In order to understand the observed damping of solitary waves in the course of their propagation, a mathematical analysis of the propagation in the still water channel of uniform rectangular section was developed.

Since the channel was horizontal, the equations of motion and continuity would be given by

$$\frac{\partial U}{\partial t} + U\frac{\partial U}{\partial x} = -\gamma U^2 - g\frac{\partial h}{\partial x} \quad \cdots\cdots(4.1),$$

$$\frac{\partial h}{\partial t} + \frac{\partial}{\partial x}(hU) = 0 \quad \cdots\cdots(4.2),$$

where γ is the coefficient of friction, while it is expressed by Manning's coefficient as follows.

$$\gamma = gn^2 R^{-\frac{4}{3}} = gn^2(\beta h)^{-\frac{4}{3}} \quad \cdots\cdots(4.3),$$

where β is the coefficient of the form of channel section and for the rectangular section,

$$\beta = \frac{1}{1+\frac{2h}{b}} \quad \cdots\cdots(4.4).$$

Putting

$$C = \sqrt{gh} \quad \cdots\cdots(4.5),$$

the well-known characteristic equations are written by

$$\frac{dx}{dt} = U \pm C \quad \cdots\cdots(4.6),$$

$$\frac{d}{dt}(U \pm 2C) = -\gamma U^2 \quad \cdots\cdots(4.7),$$

$$\gamma = g^{\frac{7}{3}} n^2 \cdot \beta^{-\frac{4}{3}} \cdot C^{-\frac{8}{3}} \quad \cdots\cdots(4.8).$$

For convenience, the characteristic curve with + sign is called "Curve I" and that with − sign "Curve II"

(i) Now, let the point at which the Curve II passing through the poiont (x_n, t_n) adjacent to the t-axis intersects the t-axis, be $(0, t)$ (refer to Fig. 14). Then equations (4.6) and (4.7) will be expressed approximately by

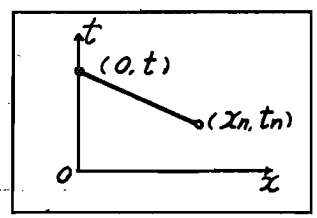

Fig. 14. x-t diagram.

$$\frac{0-x_n}{0-t_n} = \frac{U+U_n}{2} - \frac{C+C_n}{2} \quad \cdots\cdots(a),$$

$$\frac{(U-2C)-(U_n-2C_n)}{t-t_n} = -\frac{\gamma U^2+\gamma_n^2 U_n^2}{2} \quad \cdots\cdots(b).$$

If the variation in water level at $x = 0$ is given as $h\,(0,t) = F(t)$, then

$$C = \sqrt{g \cdot F(t)} \quad \cdots\cdots(4.9).$$

From (a) and (b), U becomes

$$U=\frac{B_1}{2A_1}\pm\sqrt{\left(\frac{B_1}{2A_1}\right)^2-\frac{C_1}{A_1}} \quad \cdots\cdots(4.10),$$

where

$$A_1=1-\gamma x_n,\ B_1=3C-C_n,$$

$$C_1=2C^2-CU_n-(2C_n-U_n)(C_n-U_n)-\gamma_n U_n^2\cdot x_n,$$

$$t=t_n+\frac{2x_n}{\{(C-U)+(C_n-U_n)\}} \quad \cdots\cdots(4.11).$$

Hence the values of C, U and t may be determined by the three equations (4.9), (4.10), (4.11) with the method of interpolation. γ is the function of C, as shown by equation (4.8).

(ii) When the Curve I passing through (x_m, t_m) intersects Curve II passing through an adjacent point (x_n, t_n) at the point (x, t), the following relations may by derived in the same way (refer to Fig. 15).

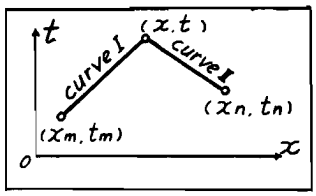

Fig. 15. x-t diagram.

$$\frac{x-x_m}{t-t_m}=\frac{U+U_m}{2}+\frac{C+C_m}{2} \quad \cdots\cdots(a'),$$

$$\frac{x-x_n}{t-t_n}=\frac{U+U_n}{2}-\frac{C+C_n}{2} \quad \cdots\cdots(a''),$$

$$\frac{(U-U_m)+2(C-C_m)}{t-t_m}=-\frac{\gamma U^2+\gamma_m U_m^2}{2} \quad \cdots\cdots(b'),$$

$$\frac{(U-U_n)-2(C-C_n)}{t-t_n}=-\frac{\gamma U^2+\gamma_n U_n^2}{2} \quad \cdots\cdots(b'').$$

If the quantities at the two points (x_m, t_m) and (x_n, t_n) are known, then x, t, U and C will be obtained. To simplify calculation, the two points are selected so as to be $t_m = t_n$. The results are

$$C=\frac{1}{8}\Big[-(U_m-U_n)\pm\sqrt{9(U_m-U_n)^2+24(U_m-U_n)(C_m+C_n)+16(C_m+C_n)^2-8(\gamma_m U_m^2-\gamma_n U_n^2)(x_n-x_m)}\Big] \quad \cdots\cdots(4.12),$$

$$U=\frac{1}{2A_2}\pm\sqrt{\left(\frac{1}{2A_2}\right)^2-\frac{B_2}{A_2}} \quad \cdots\cdots(4.13),$$

where

$$A_2=\frac{\gamma(x_n-x_m)}{2C+C_m+C_n+U_m-U_n}$$

$$B_2=2C-2C_m-U_m+\frac{\gamma_m U_m^2(x_n-x_m)}{2C+C_m+C_n+U_m-U_n},$$

or

$$B_2=-2C+2C_n-U_n+\frac{\gamma_n U_n^2(x_n-x_m)}{2C+C_m+C_n+U_m-U_n},$$

$$t=t_m+\frac{2(x_n-x_m)}{2C+C_m+C_n+U_m-U_n} \quad \cdots\cdots(4.14),$$

$$x=\frac{(x_m+x_n)C+(x_n-x_m)U+(U_m+C_m)x_m+(C_n-C_m)x_m}{2C+C_m+C_n+U_m-U_n} \cdots(4.15),$$

(iii) *Initial characteritic curve*

At the front of the disturbance. $U=0$, $C=\sqrt{gh_o}$, so by equation (4.6)

$$\frac{dx}{dt}=\pm\sqrt{gh_o} \quad \cdots\cdots(4.16),$$

where h_o is the initial still water depth.

At the boundary, the rise in water level is assumed to be linear, in other words,

$$h=at+h_o \text{ or } \zeta=at \text{ at } x=0, \quad \cdots\cdots(4.17).$$

Hence equation (4.9) becomes

$$C=\sqrt{g(at+h_o)} \quad \cdots\cdots(4.18).$$

For the sake of generalization, the following non-dimensional factors are used.

$$\sigma=\frac{a}{\sqrt{gh_o}}, \quad X=\sigma\frac{x}{h_o} \quad T=\sigma t\sqrt{\frac{g}{h_o}},$$

$$H=\frac{h}{h_o}, \quad c=\frac{C}{\sqrt{gh_o}}, \quad u=\frac{U}{\sqrt{gh_o}}, \quad \Gamma=\frac{\gamma h_o}{\sigma} \quad \cdots\cdots(4.19).$$

By these non-dimensional quantities, the characteristic equations (4.16) and (4.17) are transformed to

$$\frac{dX}{dT} = u \pm c \quad \cdots\cdots\cdots\cdots\cdots\cdots\cdots\cdots (4.20),$$

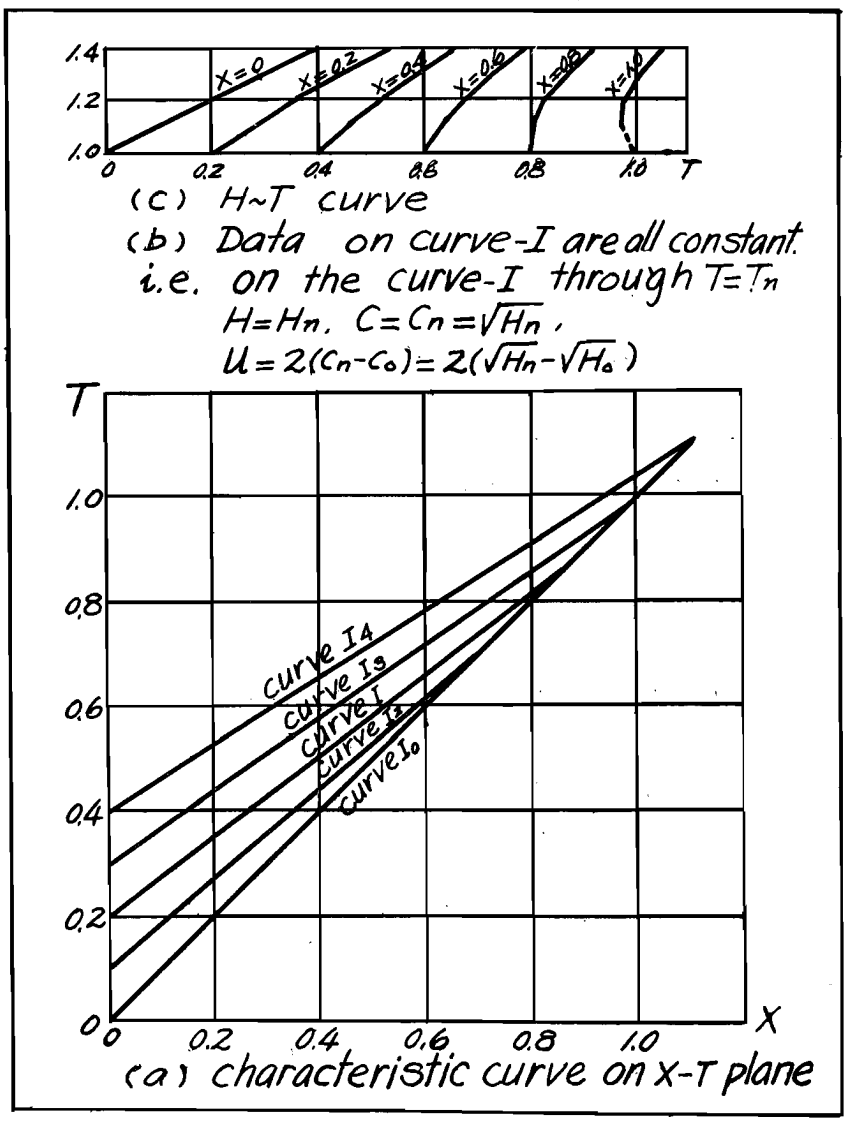

Fig. 16 (a). Example of caluculation A (case of $n=0$).
In diagram (c), ordinate is H.

$$\frac{d}{dT}(u\pm 2c)=-\Gamma u^2 \qquad \cdots\cdots\cdots\cdots\cdots\cdots(4.21).$$

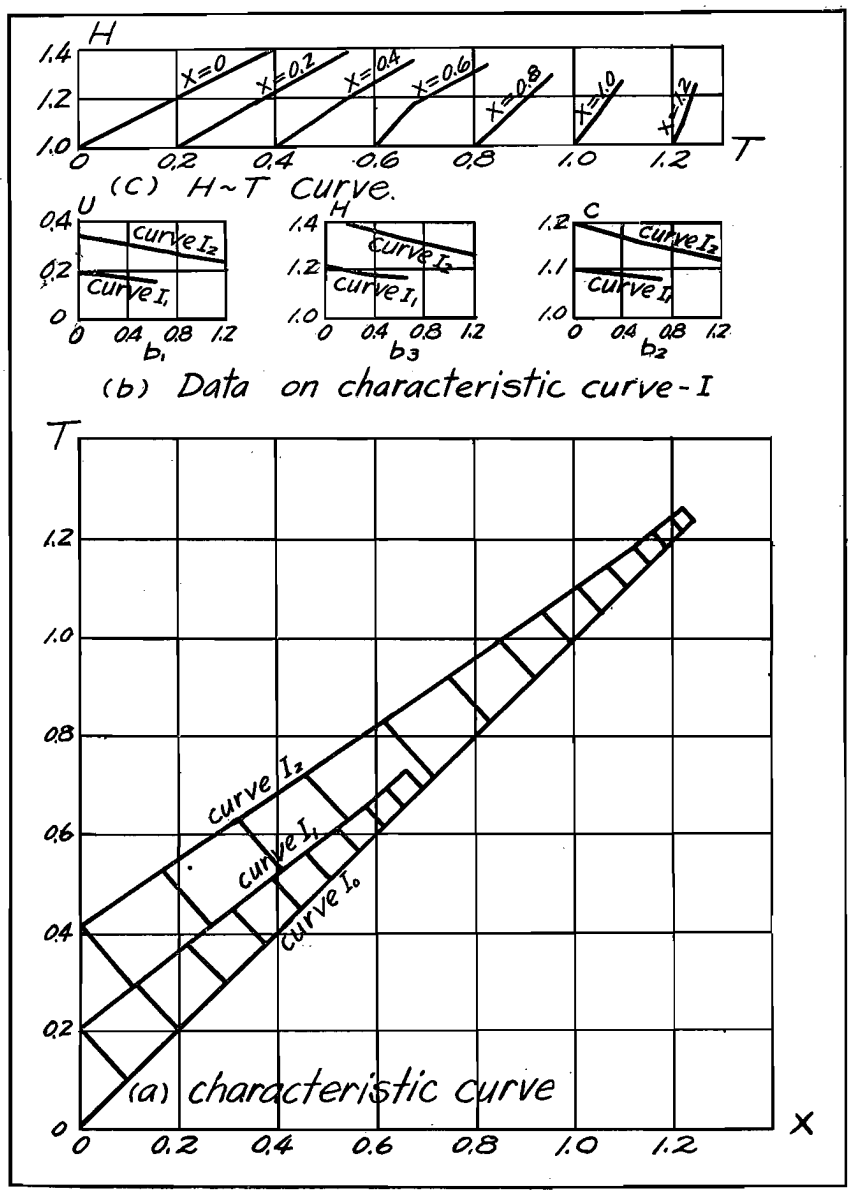

Fig. 16 (b). Example of calculation B (case of $n^2\sigma^{-1}h_0^{-1/3}=2.77\times10^{-3}$, $h_0/b=0.2$). In diagrams (b), abscissas are X.

Hence the following calculations are made in quite same menner as in the former method. The non-dimensional factor Γ corresponding to frictional resistance expressed by equation (4.8) is now given by

$$\Gamma = gn^2\sigma^{-1}h_0^{-\frac{1}{3}}\beta^{-\frac{4}{3}} \cdot c^{-\frac{6}{3}} \quad \cdots\cdots(4.22)$$

for the rectangular sectional channel and $\beta = 1/\left(1+\frac{2h_0}{b}c^2\right)$, and the boundary conditions are, from equations (4.17) and (4.18),

$$H = T+1 \text{ or } c=\sqrt{T+1} \text{ at } X=0 \quad \cdots\cdots (4.23).$$

The calculation is very troublesome, but in the case of (ii), it can be carried out mechanically, or by the use of a nomograph, so that the labour and the time may be minimized.

For the case of $h_0/b = 0.2$, i. e. $\beta = 1/(1+0.4c^2)$, some examples are shown in Fig. 16 (a) and (b), and also summarized in Fig. 17 (other diagrams are omitted in this paper).

The experimental results obtained in the channel, shown in Fig. 13, are illustrated in Figs. 18 and 19.

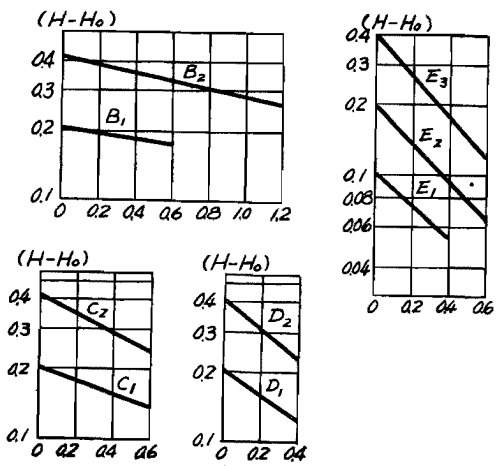

Fig. 17. Calculation of wave damping.

abscissa ; $\varkappa = \frac{\sigma}{h_0}x$, ordinate ; $\log(H-1) = \log \zeta/h_0$

This set of curves is one of the groups of the characteristic curves on the x-t plane.

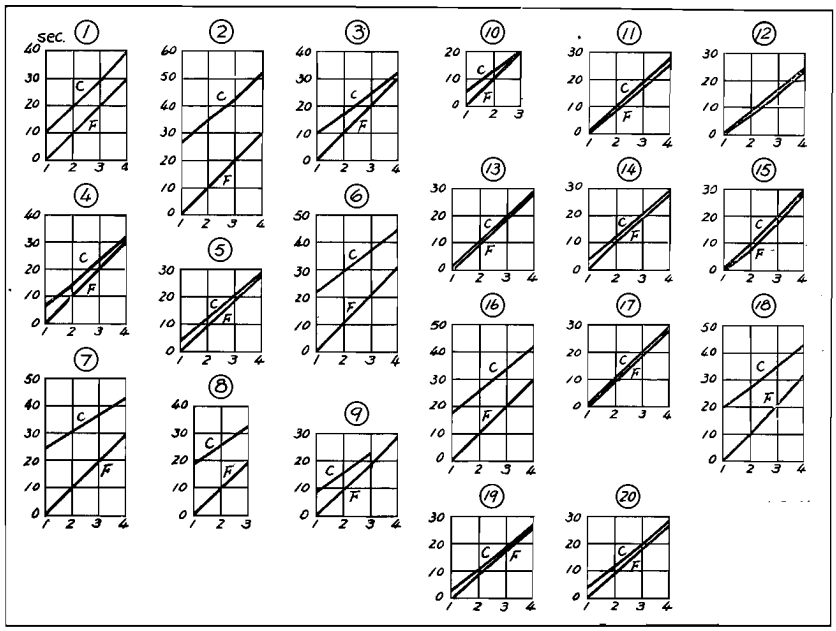

Fig. 18. Propagation velocity of wave front and peak (vert. axis : time of concentration, hor.axis : distance, F · front, C : peak).

The propagation velocity at the wave front is 43.8 cm/sec at the still water depth h_o = 2.0 cm and nearly coincides with the theoretical value $C=\sqrt{gh_o}$ = 44.3 cm/sec.

Though the propagation velocities at the crest of the wave differed from each other, they were generally higher than the propagation velocities at the wave front. The same tendency can be obtained by calculation of the characteristic curves, and the results of measurement agreed with the theoretical calculation.

For example, the example B in Fig. 16 corresponds to the means of Experiments No. 4 and 14.

Next, define the damping coefficient α by the following equation,

$$\zeta_{max}=\zeta_{omax}\cdot e^{-\alpha x} \quad \text{or} \quad \alpha=-\frac{ln\ \zeta_{max}-ln\ \zeta_{omax}}{x} \qquad \cdots\cdots\cdots\cdots \quad (4.24)$$

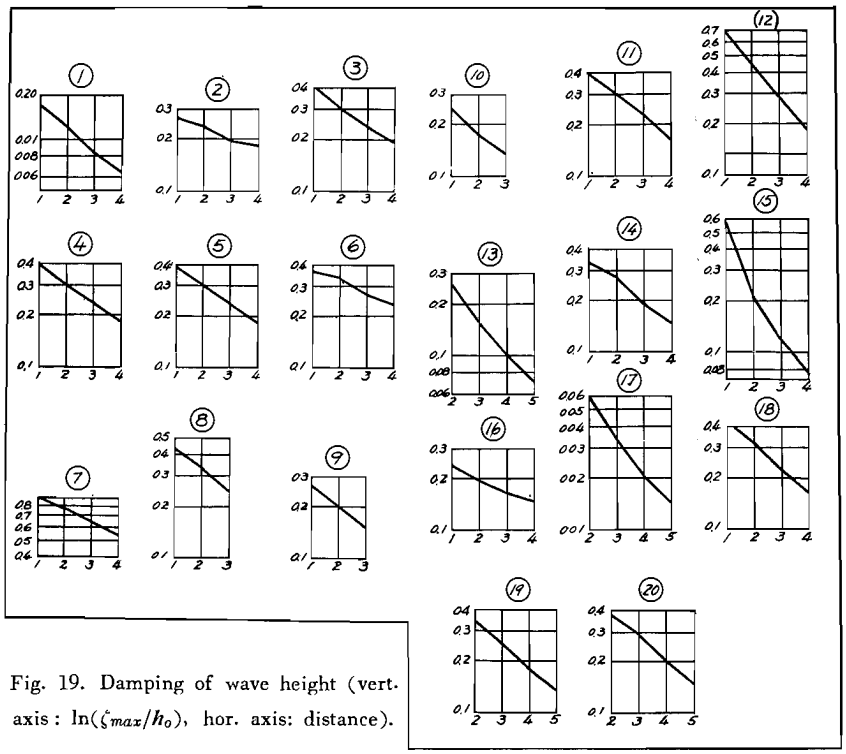

Fig. 19. Damping of wave height (vert. axis : $\ln(\zeta_{max}/h_0)$, hor. axis: distance).

where, ζ_{max} = maximum wave height at the point x

ζ_{omax} = maximum wave height at $x = 0$

x = distance from zero point.

The dimension of α is $[L]^{-1}$.

Let A be the non-dimensional expression of α, then

$$|H-1|_{X=X} = |H-1|_{X=0} \cdot e^{-AX}$$

or

$$A = -\frac{1}{X}\left\{ ln|H-1|_{X=X} - ln|H-1|_{X=0} \right\} \quad \cdots\cdots\cdots(4.25),$$

namely

$$A = \frac{h_0}{\sigma}\alpha \quad \cdots\cdots\cdots(4.26).$$

Since the experimental and calculated values (Figs. 17 and 19) of the

maximum wave height coincide well on the logarithmic curves. it may be considered that the damping coefficient α, defined by equation (4.24), can represent the mode of disturbance-distorsion. The quantity defined by $\sigma = \frac{a}{\sqrt{gh_o}}$ is referred to as "steepness"

Assuming that the form of the wave is of the linear type, that is

$$a = \frac{\zeta_{omax}}{t_{oc}} ,$$

where t_{oc} means the time required for the maximum wave height at $x = 0$, and with Manning's coefficient being $n = 1.4 \times 10^{-2}$, the values of σ and α for $h_o = 2.0$ cm were calculated and tabluated in Table 1 and also illustrated graphically in Fig. 20.

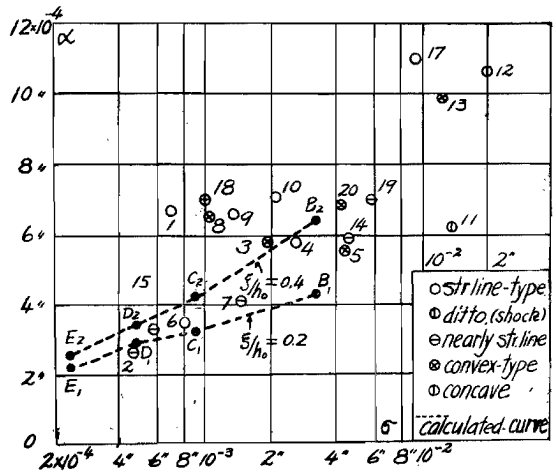

Fig. 20. Steepness σ and damping coefficient α.

From the $\sigma - \alpha$ diagram, it can be concluded that α is proportional to σ, namely that steeper wave has the tendency to damp more quickly. If β is constant, the value of $n^2\sigma^{-1}h_o^{-\frac{1}{3}}$ is one of a parameter to express the wave-mode. Graphical representation of the relation between the parameter $n^2 \cdot \sigma^{-1}h_o^{-\frac{1}{3}}$ and damping coefficient A is given in Fig. 21. As seen from this curve, A increases with the value of $n^2\sigma^{-1}h_o^{-\frac{1}{3}}$, therefore A decreases with the increase of σ. Since $A = \frac{h_o}{\sigma}\alpha$, the decrement of the value of A does not necessarily mean the decrement of α, but α rather increases with σ.

$n^2\sigma^{-1}h_0^{-\frac{1}{3}}$ (cgs)	u ($m^{\frac{1}{3}}\cdot sec$)	h_0 (cm)	σ	x (cgs)	t (cgs)	H-1 $_{x=0}$	A	α	remarks
2.77×10^{-3}	1.4×10^{-2}	2	3.19×10^{-3}	$1.60\times10^{-3}x$	$7.07\times10^{-2}t$	0.414 0.203	0.393 0.260	6.29×10^{-4} 4.16 //	case of
7.70 //	//	2	9.40×10^{-4}	$4.70\times10^{-4}x$	2.08 //	0.411 0.202	0.89 0.66	4.18 // 3.10 //	$\frac{h_0}{b}=0.2$
1.51×10^{-2}	//	2	4.20 //	2.41 //	1.06 //	0.410 0.202	1.45 1.20	3.48 // 3.88 //	$A=-\frac{\ln\Delta\lvert H-1\rvert}{\Delta x}$
3.08 //	//	2	2.35 //	1.18 //	5.19 //	0.401 0.200	2.13 1.88	2.51 // 2.22 //	$=\frac{ho}{\sigma}\alpha$
						0.100	1.54	1.82 //	

Table 1. The value of damping coefficient obtained by the method of characteristic equation.

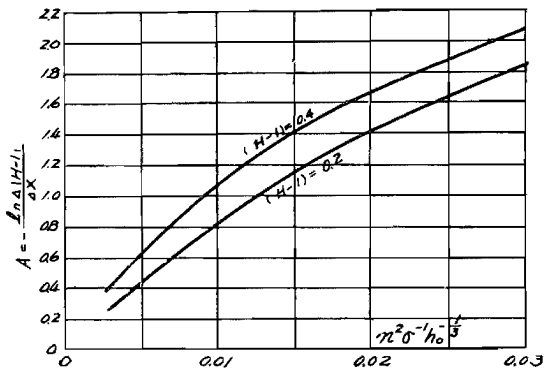

Fig. 21. $n^2\sigma^{-1}$ $ho^{-1/3}$—A diagram ($ho/b=0.2$).

4.2. The Second Preliminary Experiment (experiment for the law of similitude)

In the previous chapter the artificial roughness of the model was studied, but in this case the actual data of the observed coefficient of roughness in the Osaka estuary were not yet clearly known.

Therefore it was somewhat uncertain whether the similitude was really established or not. Hence a second preliminary experiment was carried out to clarify this point. The channel used in this experiment was a steel channel of 20.0 cm width, 15.0 cm height and 20.0 m length. For the initial still water depth 2.0 cm and 4.0 cm, and for the geometrically similar wave of wave height 5 mm and 10 mm, the deformation and damping of translation

waves under various artificial roughness were studied.

The wave generator used in the second preliminary experiment was of the same type as that in the first experiment but improved (Fig. 22), with a screw spiral and synchronous motor.

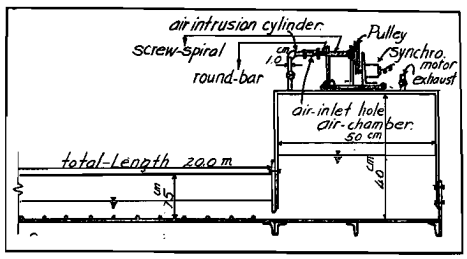

Fig. 22. Experiment channel and pneumatic wave generator.

In the case where the channel is very long, compared with the wave velocity, the equations discussed in 2.2, for determining the dimension of the air intrusion hole, are no longer valid.

Assuming the generated wave to be a long wave,

$$U_w = \zeta \sqrt{\frac{g}{h_o}} \quad \cdots\cdots\cdots\cdots\cdots\cdots\cdots\cdots \quad (4.27)$$

then

$$Sa = \frac{A_1 h_o \left(1 + \frac{\zeta}{h_o}\right) \frac{\zeta}{h_o}}{\sqrt{\frac{\eta_o}{h_o} - \left\{\frac{\zeta}{h_o} + A_2 \sqrt{h_o} \cdot T \int_o^\tau \left(1 + \frac{\zeta}{h_o}\right) \frac{\zeta}{h_o} d\tau + A_3 \left(\frac{h_o}{d}\right)^2 \times \left(1 + \frac{\zeta}{h_o}\right)^2 \left(\frac{\zeta}{h_o}\right)^2\right\}}} \quad \cdots\cdots\cdots\cdots\cdots\cdots\cdots\cdots \quad (4.28)$$

where

$$A_1 = \frac{b}{C_a}\sqrt{\frac{\rho_a}{2\rho_w}}, \quad A_2 = \frac{\sqrt{g}}{L}, \quad A_3 = \frac{1}{2C_w^2}, \quad \tau = \frac{t}{T}, \quad \cdots(4.29)$$

S_a = cross sectional area of air intrusion hole,
ρ_a = density of air,
ρ_w = density of water,
h_o = initial water depth,
ζ = variation in water depth in channel,
T = period of wave,
η_o = difference of initial water level between air chamber and outside channel,
b = width of channel (equal to width of air chamber in this

case),

d = height of opening hole, connecting air chamber and channel,

L = length of air chamber,

C_a = coefficient of intrusion of water,

C_w = coefficient of outflow of water.

It is seen from this equation, that, in order to obtain a geometrically similar wave form corresponding to the various values of initial water depth h_o, S_a is to be chosen as proportional to h_o, if only the values of η_o/h_o, $\sqrt{H_o}\cdot T$, and h_o/d are always constant.

Though in this experiment these theoretical relationships were not completely satisfied because of the imperfect airtightness of the air chamber and of the variability of the intrusion coefficient. But any desired wave form could be obtained anyhow, by adjusting the intrusion hole. The experimental conditions and dimensions of the general plant are illustrated in Table 2.

No. of Exp.	Initial water depth: h_o	Period : T	Wooden segment height: k	Wooden segment width: t	Pitch: s	Remarks
I_1	2(cm)	45(sec)	5(mm)	5(mm)	5(cm)	$\frac{x_1}{x_2}=1, \frac{h_1}{h_2}=\frac{1}{2}$
I_2	4	32	10	5	10	
I_2'	4	32	5	5	5	$\frac{t_1}{t_2}=1.406=\left(\frac{x_1}{x_2}\right)\left(\frac{h_2}{h_1}\right)^{\frac{1}{2}}=1.414$
II_1	2	65	5	5	5	$\frac{x_1}{x_2}=1, \frac{h_1}{h_2}=\frac{1}{2}$
II_2	4	45	10	5	10	
II_2'	4	45	5	5	5	$\frac{t_1}{t_2}=1.444=\left(\frac{x_1}{x_2}\right)\left(\frac{h_2}{h_1}\right)^{\frac{1}{2}}=1.414$

Table 2. Data of the second preliminary experiment.

The experimental results are shown in Figs. 23 (a), (b) and (c) and also Figs. 24 (a), (b) and (c).

The damping of the maximum wave height is illustrated in Figs. 25 and 26.

From these diagrams, it is clear that the deformation and damping of the translation wave in the experiments I_1 and I_2 (or II_1 and II_2), are somewhat similar, but in the experiments I_1 and I_2' (or II_1 and II_2'), they are quite different. In other words, the similitude between the case where $h=2.0$ cm, b = 20.0 cm, wooden ridge 5×5 mm and that where $h=4.0$cm, b=2.0 cm, wooden ridge 10×5mm is established.

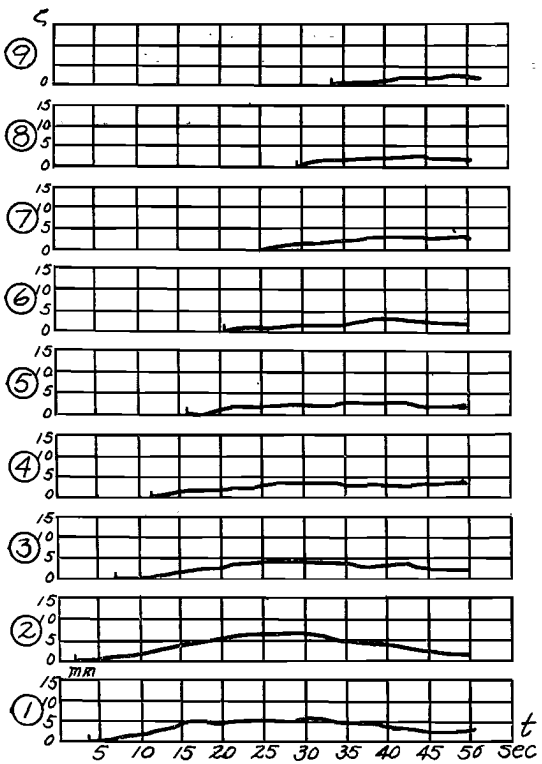

Fig. 23(a). 2nd preliminary exp. I_1 (h_o=2cm, T=45sec, k=5mm, S=5cm).

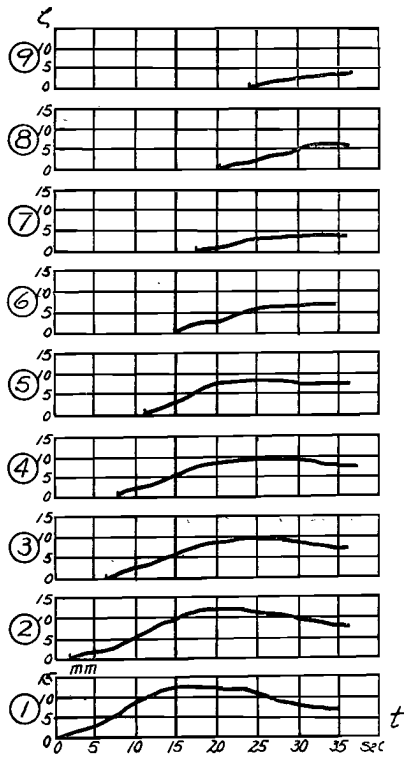

Fig. 23 (b). 2nd preliminary exp. I_2 (h_o=4cm, T=32sec, k=10mm, S=10cm).

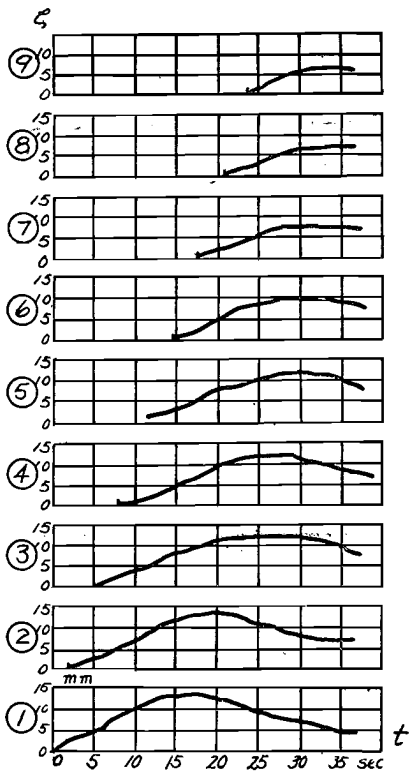

Fig. 23 (c). 2nd preliminary exp. I_2'(h_o=4cm, T=32sec, k=5mm, S=5cm).

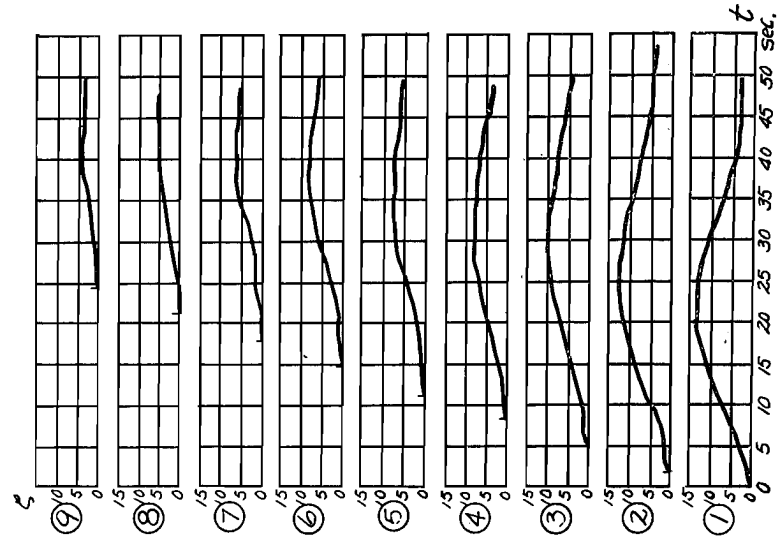

Fig. 24 (b). 2nd preliminary exp. II_2
($h_o=4$cm, $T=45$sec, $k=10$mm,
$s=10$cm).

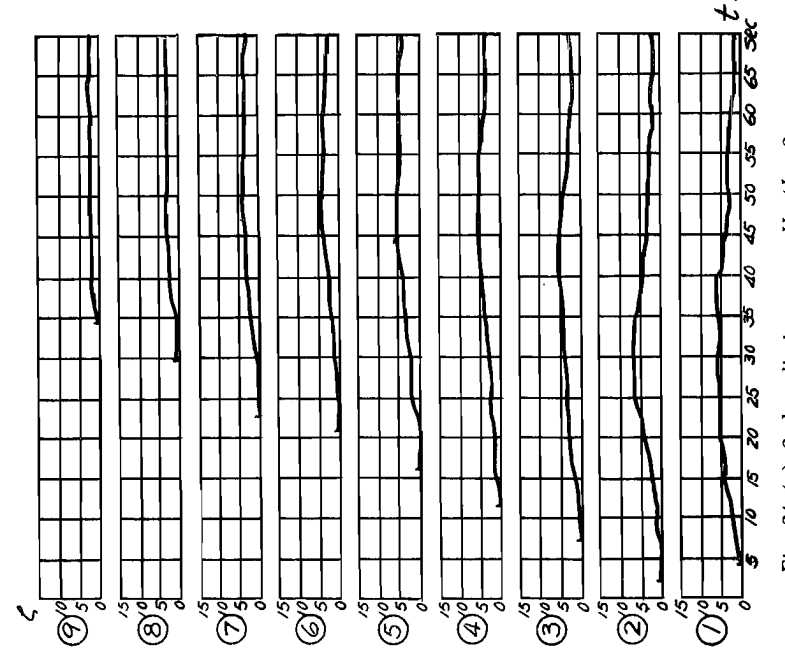

Fig. 24 (a). 2nd preliminary exp. II_1 ($h_o=2$cm,
$T=65$sec, $k=5$mm, $s=5$cm).

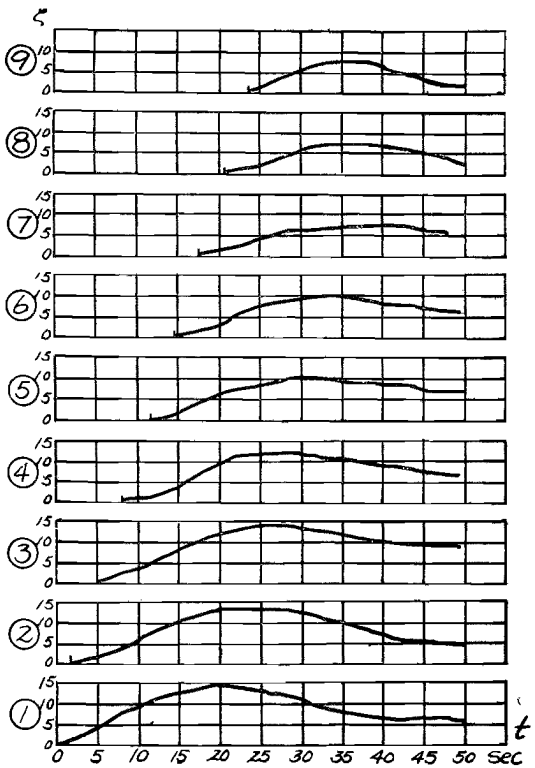

Fig. 24 (c). 2nd preliminary exp. II_2' (H_0=4cm, T=46sec, k=5mm, s=5cm).

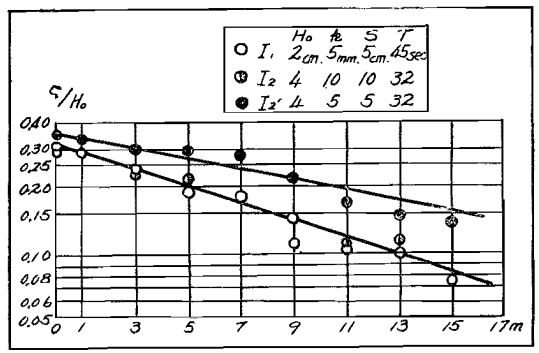

Fig. 25. Damping of maximum wave height in exp. I.

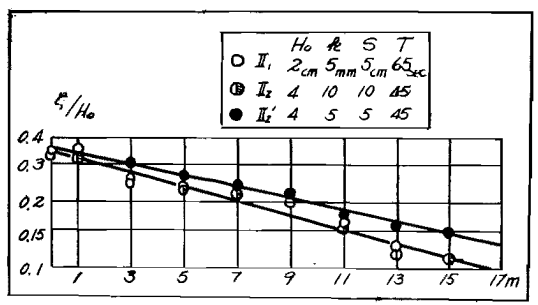

Fig. 26. Damping of maximum wave height in exp. II.

As described in 2.3, to satisfy the similitude between two channels, the following conditions are necessary

$$\frac{k_{s2}}{R_2} = q\left(\frac{k_{s1}}{R_1}\right)^p \quad \cdots\cdots\cdots\cdots\cdots\cdots \quad (4.30),$$

where

$$p = \left(\frac{R_2}{R_1}\right)^{-\frac{1}{4}} \left(\frac{x_1}{x_2}\right)^{-\frac{1}{2}}$$

and

$$q = exp\ x\{A_{ro}\ (1-p) + (\delta_2 - p\delta_1)\}.$$

In the present case $x_1/x_2 = 1$, $h_1/h_2 = 1/2$ (corresponding to the initial water depth $h_o = 2.0$ cm, 4.0 cm).

Neglecting the condition factor δ and taking the values $x = 0.4$, $A_{r2} = 6.0$, the relation (4.30) is plotted in Fig. 27.

As described in 2.3, the value of k_s is generally largest in the case of $s/k = 10$ and, as shown in Fig. 8, the value of k_s/k is 5.

Since $s = 10\ k$ in these experiments,

$k_{s1} = 5\ k_1 = 25.0$mm,

$k_{s2} = 5\ k_2 = 50.0$mm.

The value of k_{s2} corresponding to $k_{s1} = 25$ mm is comparatively large and amounts to $k_{s2} = 6.5 \sim 6.8$ mm, as shown in Fig. 27. Nevertheless, the equation of similitude expressed by equation (4.30) is considered to hold almost perfectly due to the reasons described below.

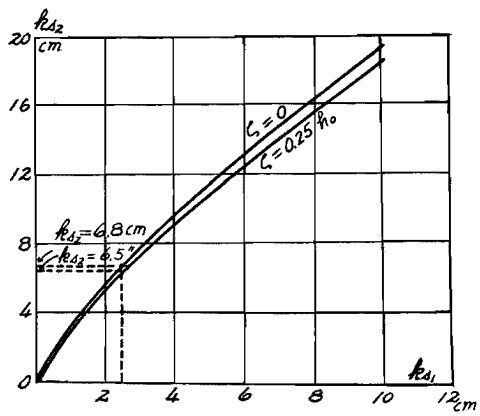

Fig. 27. Theoretical values of k_{s2}.

(1) The value of k_{s2}/k_2 is slightly larger than k_{s1}/k_1 because $t_1/k_1 = 1$ and $t_2/k_2 = 1/2$.

(2) Ratio of the height of wooden ridge to the hydraulic mean depth is comparatively large ($R_1/k_1 = 3.3$ and $R_2/k_2 = 2.7 \sim 2.9$) and is nearly equal to the critical point ($R/k < 3.0$) where the effect of the free

surface can not be neglectd.

It may be inferred that if the height of the wooden ridge is too great, the free surface effect can not be neglected. According to the report of Corps of Engineers, U.S.Army,[7] the same conclusion may be obtained, as shown in Fig. 28, for log $R/k < 5$ (i.e. $R/k < 3$) in the case of a concrete ridge of right triangular section. Though in this case the form of the wooden ridge is triangular and the value of k_s/k is comparatively large, a necessary correction is suggested, if the height of the ridge is above a certain limit. In the present experiments, since the value of R/k was sufficiently large, it is believed that the calculation as deseribed in 2.3 is quite satisfactory.

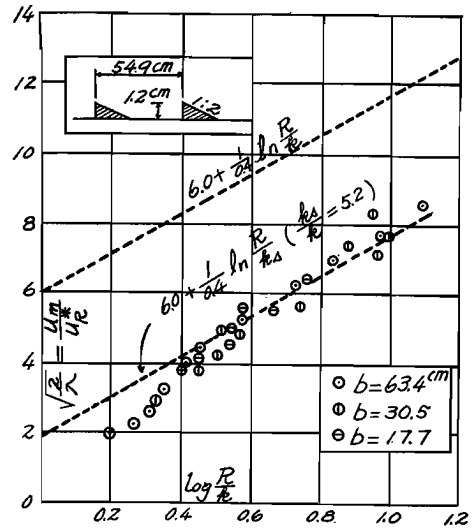

Fig. 28. Relation of artificial roughness and coefficient of friction.

5. Experimental Results

5.1. Measuring Stations and Experiment Waves

65 points were selected as the measuring stations in the model as shown in Fig. 29.

Since an electromagnetic oscillograph with 16 elements was used for measuring the water level, simultaneous measurement at these points was impossible. Hence, generating a wave of identical form repeatedly, the water level was recorded at several points each time and each wave was identified by comparing the value obtained at one fixed point situated at measuring point (1) (Fig. 29). By this method, it was recognized that in almost all cases the waves were perfectly identical with the others.

The wave form, adopted in this experiment, was that of the tsumami caused by the "Jane-typhoon" as shown in Fig. 30, but experiments for longer and shorter periods were also made in order to investigate the ef-

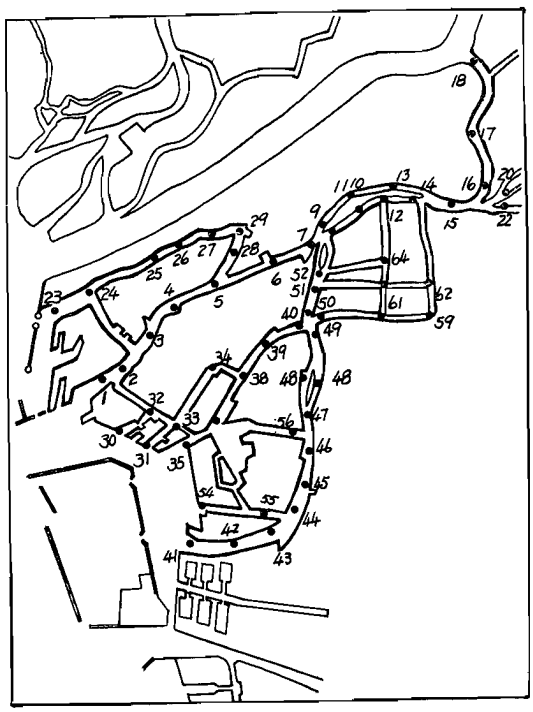

Fig. 29. Measuring stations in model.

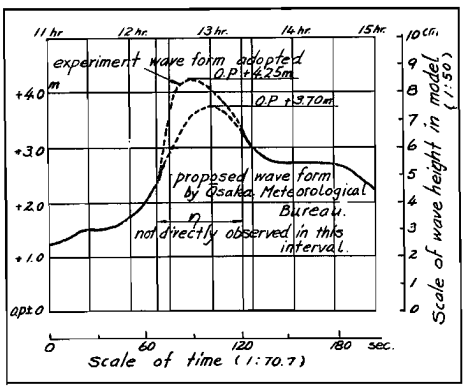

Fig. 30. Standard form of experimental wave.

fects of different wave forms.

The normal initial water level before the generation of the meteorological bore was O.P. + 1.25 m (model dimension + 25 mm). However, considering the worst condition that the highest tide and the meteorological bore occur simultaneously, experiments for the case of an initial water depth of O.P.+2.00m (model type + 40 mm) were also made.

The model scale was 1/500 in the horizontal and 1/50 in the vertical,

and the time scale was

$$\frac{t_2}{t_1} = \frac{x_2}{x_1}\left(\frac{h_2}{h_1}\right)^{\frac{1}{2}} = \frac{1}{70.7}$$

An actual record of the tsunami caused by the "Jane-typhoon" is lacking for the peak and its proximity, so that no information on the maximum value of the water level is available. The Osaka Meteorological Bureau estimated it to be about O.P. + 3.70 m, but according to other observers, it was estimated to be about O.P + 4.20 m. In this experiment, the latter value was used as the worst case.

5.2. Experimental Results

The experiment was made mainly for the variation in water level, and partially for the wave-velocity. Some results are shown in Figs. 31~35.

The unit in these diagrams is that used in the model experiment. Comparing the case of initial water level of + 25mm (O.P. + 1.25 m) with + 40mm (O.P. + 2.00m), it was observed that the damping in the former case was slightly larger than in the latter. It may be due to the fact that the effect of roughness was smaller in the latter case because of the water depth being deeper (so, smaller value of k_s/R as predicted in 2.3).

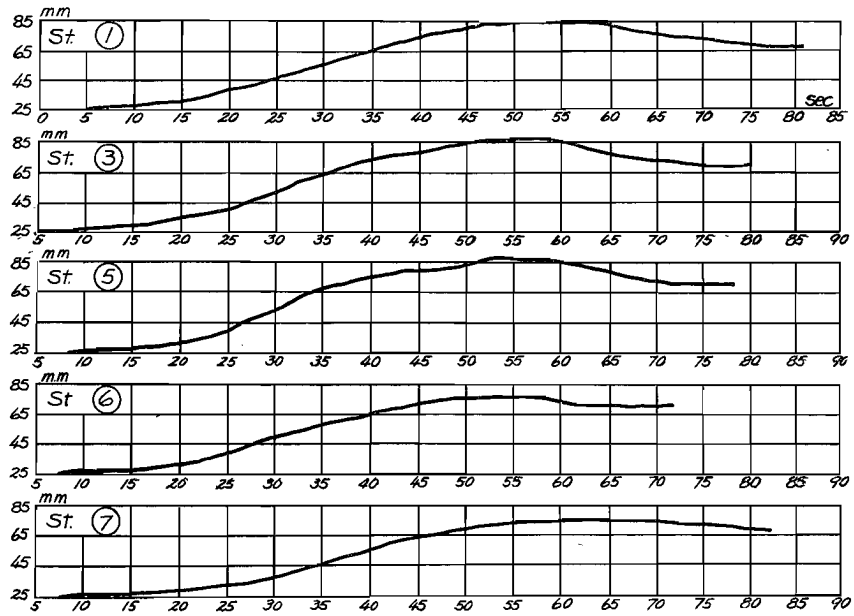

Fig. 31 (1). Experimental hydrograph in Aji-River.

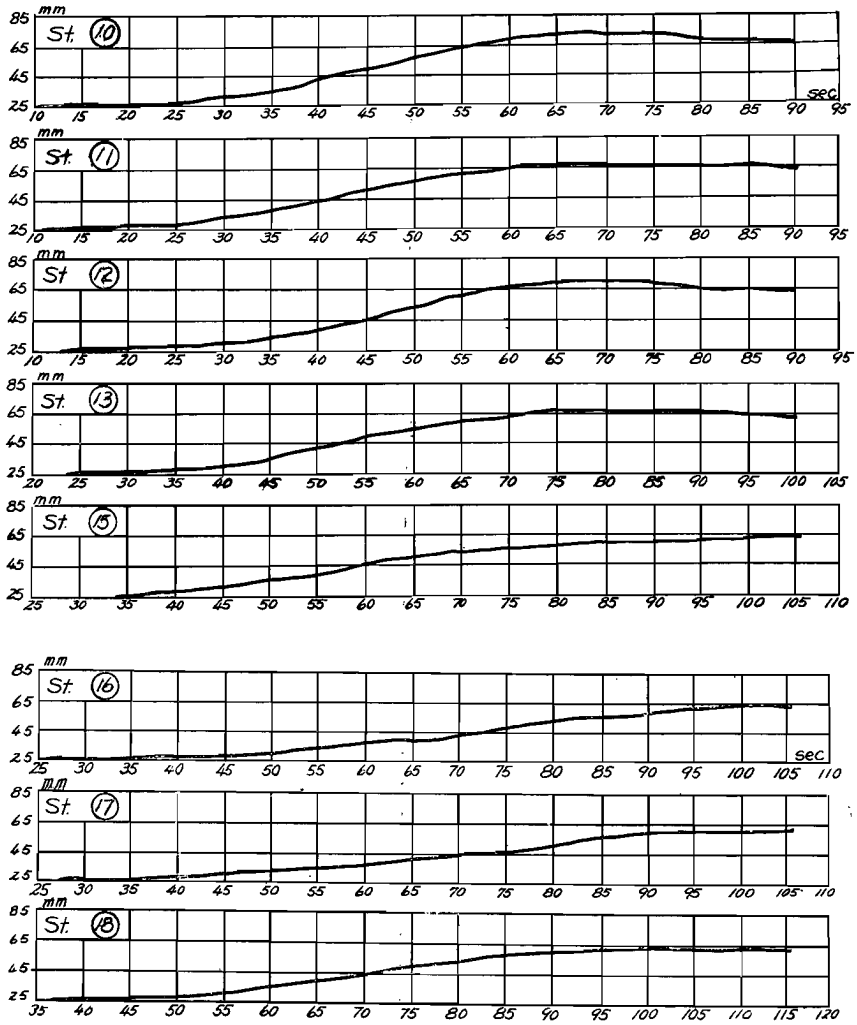

Fig. 31 (2). Experimental hydrograph in Aji-River.

However, compared with the effect of wave form, this effect is so small that it is negligible.

(*1*) *On the characteristics of each river*

(*a*) *Aji River*, (*Aji River. Tosabori River, Dojima River and Old Yodo River*)

These rivers will be divided into the following four sections : (Figs. 32,

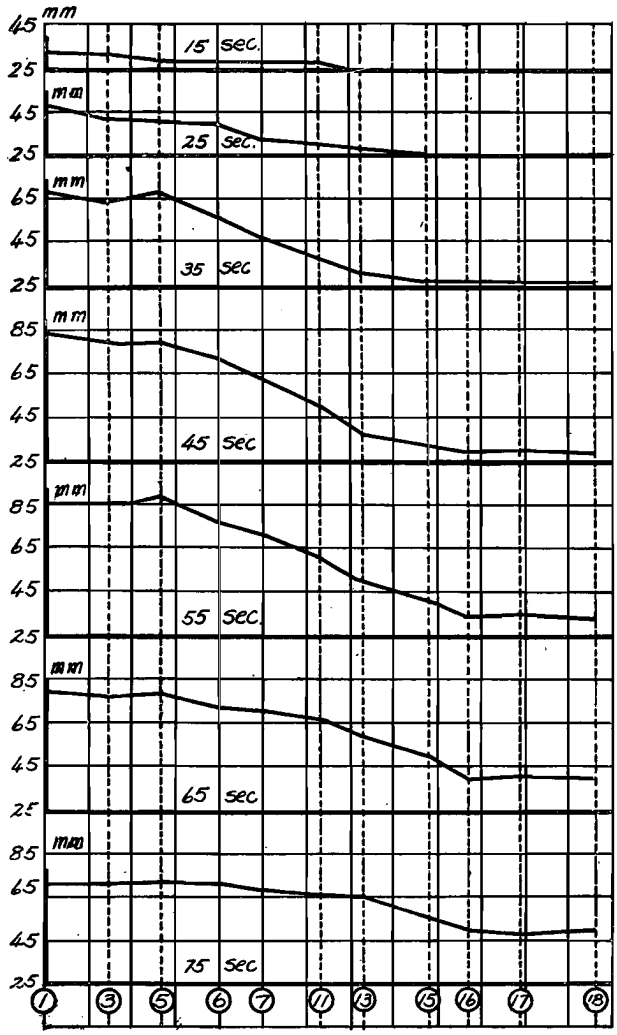

Fig. 32. Wave profile in Aji-River (case of initial water level O.P.+1.25m).

33 and 34).

From station (1) to (5).

This section belongs to the Osaka inland harbour and hence the river is very wide. Since it is abruptly necked at the upper part, the wave propagation is checked. The highest wave height in this section is nearly equal at every point and there is no damping. Even a slightly greater elevation is

seen at the upper part.

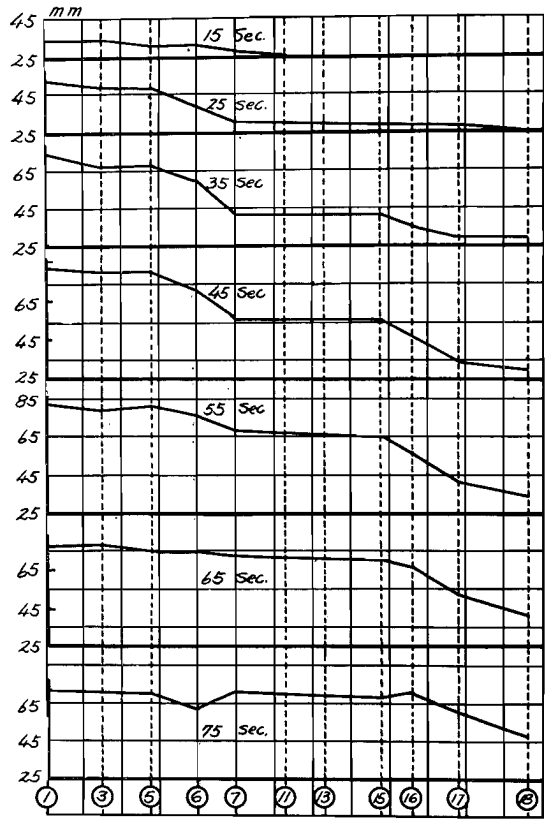

Fig. 33. Wave profile in Aji-River (case of initial water level O.P. +2.00m).

From station (5) to (16).

In this section the channel is straight and constant in width, so the damping is clearly recognized.

From station (7) to (16).

In this section the channel is also vary uniform and, owing to its closure at the Kema-Lock, the water of this whole section oscillates as a tank-oscillation by reflection. As this section is considered to lie just at the node of oscillation, the damping is subsequently small. At the confluence of Tosabori River and Dojima River, the water level is slightly increased.

(*b*) *Shorenji River* (*including Rokkenya River*)

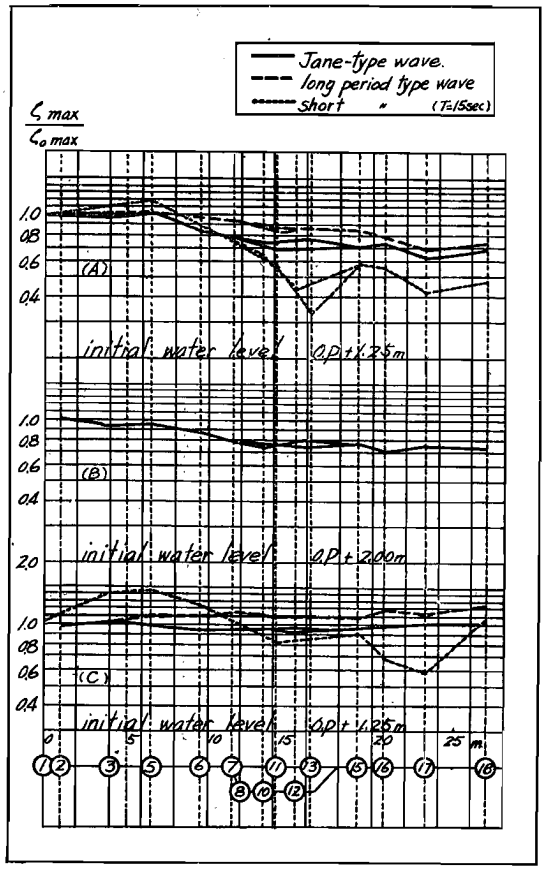

Fig. 34. Damping of maximum wave height (A and B : artificially simulated, C : not simulated).

This river bends at point (29). The water level increases uniformly, especially at the bending point (29), by reflection.

(*c*) *Shirinashi River* (*incldíng Dotonbori River and East Yokobori River*)

These rivers can be divided into the following three sections :

From station (35) to (40), i.e. Shirinashi River.

Because of the narrow channel in this section, especially in the upstream portion, the damping of the wave is very gentle. In the case of the mortar finished model channl, the wave height at the upper part was rather higher.

From staton (40) to (59), Dotonbori River.

Since it is a uniform and straignt channel, the damping is remarkably clear. But due to its abrupt bending at point (59) the effect of reflection is to be seen asslight at this point.

From station (59) to (65), East Yokobori River.

Because it is also a uniform and straight channel, the damping is clear.

(*d*) *Kizu River*

This river is also divided into the following three sections:

From station (41) to (45).

In this siction, the width of the river becomes gradually narrow so that no damping can be seen.

From station (45) to (40).

Since the river width of this section becomes narrow upstream, the damping is not remarkable.

From station (40) to (53).

Because of its uniform section and straight channel, the wave is clearly damped.

(*2*) *Variation in velocity*

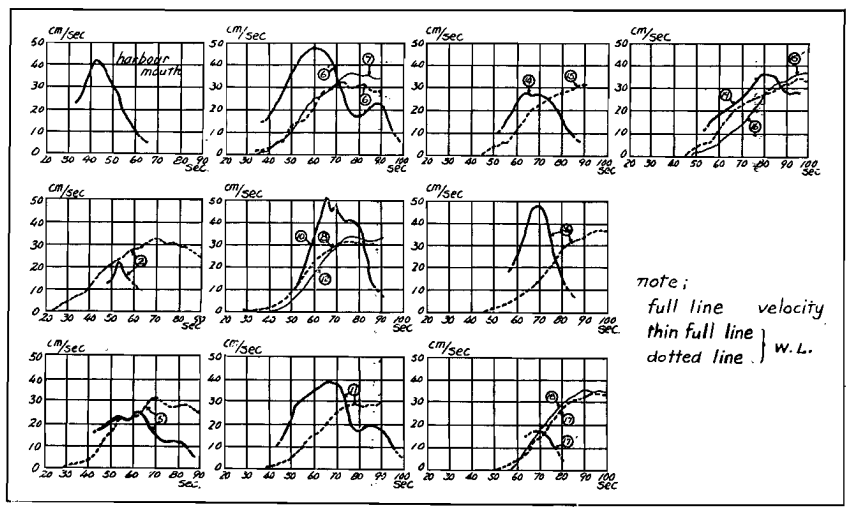

Fig. 35. Observed velocity diagram in Aji River.

Fig. 35 illustrates the velocity variation in the mortar finished model of Aji-River, for which the artificial increase of roughness was not taken into consideration. The maximum value of velocity occurs earlier than the highest water level. It appears when the slope of uprising water level is steepest, and it attains the maximum value of nearly 50 cm/sec at the narrowest section.

6. Conclusion

In experimental studies on meteorological tsunamis traveling up the estuaries, it is very important (as in many other model experiments) to secure a similitude between prototype and model. The factors governing the damping of a traveling bore, which was the main object of this experiment, are the characteristics of the wave itself and the condition of the channels.

One of ruling factors for the damping of waves is the frictional resistance, i. e. the roughness of a channel. And a similitude could be established by the use of proper devices of artificial roughness, as described in paragraphs 2.3 and 4.2.

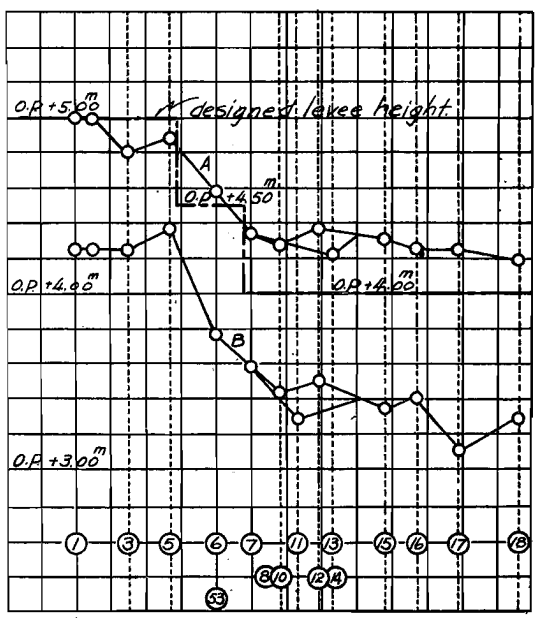

Fig. 36. Observed maximum water level and designed levee height for Aji-River.

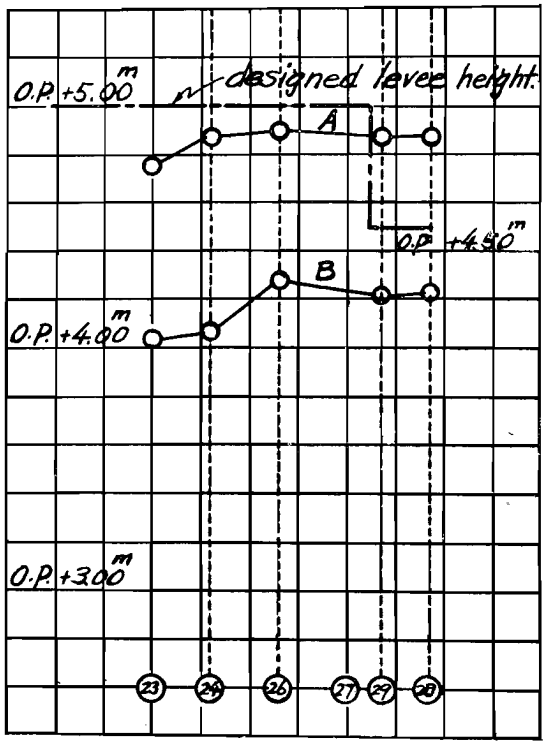

Fig. 37 Observed maximum water level and designed levee height in Shorenji River.

In this experiment, there were two points which seemed to be imperfect and not strictly valid, the one was the assumption of the Manning coefficient $n=0.03$ and the other was the presumption of equivalent sand roughneess.

Such other factors as proper stream flows, wind waves and density currents had to be considered. But the proper stream flows of these rivers are very slow because of their flat bed, and the effects of wind waves and density currents did not seem to be remarkable.

As these factors do not contribute to an increase in wave heights but rather to their reduction, it is safer to neglect these factors in determining the designed height of embankments which would prevent tsunamis. The greatest wave height at each of the measuring stations is tabulated in Table 3 and comparison with the designed height of the levees now under construction, are shown in Figs. 36, 37, 38 and 39.

From these diagrams, it may be concluded that the embankment now

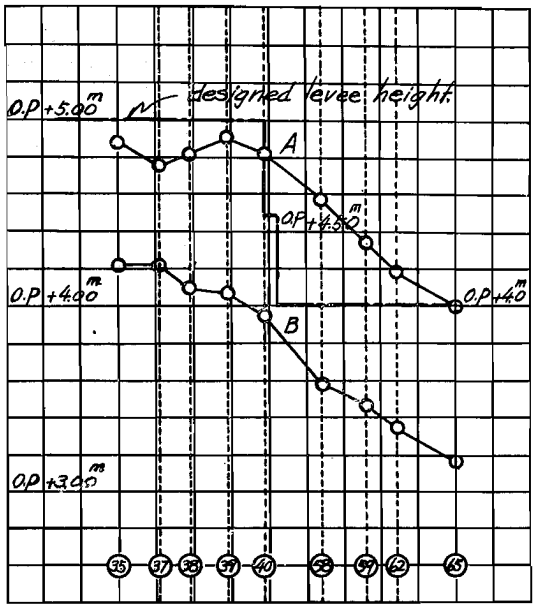

Fig. 38. Observed maximum water level and designed levee height in Shirinashi, Dotonbori and East Yokobori River.

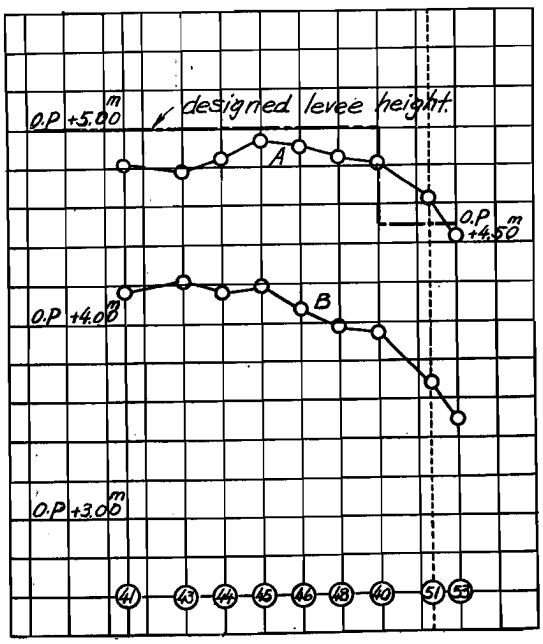

Fig. 39. Observed maximum water level and designed levee height in Kizu River.

River	No. of Station	Name of Station	O. P. +1.25m Initial Water Level		O. P. +2.00m Initial Water Level	
			Max. W.L.	Ratio to St.(1)	Max. W. L.	Ratio to St. (1)
			O. P.		O. P.	
	1	Tempozan	4.25m	1.00	5.00m	1.00
	3	Ishida chyo	4.25	1.00	4.79	0.93
Aji R.	5	Rokken-chyo	4.37	1.04	4.88	0.96
	6	Genpei-watasi	3.77	0.84	4.58	0.86
	7	Kawaguchi-chyo	3.59	0.78	4.34	0.78
	8	Minato-Bridge	3.77	0.84	—	—
Dojima R.	10	Tosabori-Bridge	3.44	0.73	4.28	0.76
	11	Tamae-Bridge	3.29	0.68	—	—
Tosa R.	12	Higo-Bridge	3.50	0.75	4.37	0.79
	13	Oe-Bridge	3.32	0.69	4.22	0.74
	15	Temma-Bridge	3.35	0.70	4.31	0.77
	16	Tunajima-chyo	3.41	0.70	4.25	0.75
Old Yodo R.	17	Gempachi-Bridge	3.11	0.62	4.25	0.75
	18	Kema-Bridge	3.29	0.68	4.19	0.73
Neya R.	19	Neyagawa-Bridge	3.20	0.65	4.13	0.71
	20	Shinkita-chyo	3.23	0.66	4.04	0.68
	23	River mouth	4.04	0.93	4.76	0.92
	24	Tuneyoshi-chyo	4.07	0.94	4.88	0.96
Shorenji R.	26	Okijima-chyo	4.28	1.01	4.89	0.96
	29	Nezumijima	4.22	0.99	4.87	0.96
Rokkenya R.	28	Asahide-Bridge	4.19	0.98	4.87	0.96
	35	River mouth	4.22	0.99	4.88	0.96
	37	Kitaokajima 3-chyome	4.22	0.99	4.76	0.92
Shirinashi R.	38	Jimpei-Bridge	4.10	0.95	4.82	0.94
	39	Kitaizumi-chyo	4.07	0.94	4.97	0.97
	40	Iwamatsu-Bridge	3.95	0.90	4.82	0.94
Dotonbori R.	58	Fukasato-Bridge	3.59	0.78	4.58	0.86
	59	Yamato-Bridge	3.47	0.74	4.34	0.78
West-Yokobori R.	61	Uwatsugi-Bridge	3.44	0.73	4.19	0.73
East-Yokobori R.	62	Sueyoshi--Bridge	3.35	0.76	4.01	0.67
	65	Ima-Bridge	3.17	0.64	—	—
	41	River mouth	4.16	0.97	4.82	0.94
	43	Fujinagata	4.22	0.99	4.79	0.93
	44	Senbonmatsu	4.16	0.98	4.85	0.95
	45	Hiraohamachyo	4.16	0.98	4.94	0.95
Kizu R.	46	Chidorihama-dori	4.07	0.94	4.91	0.97
	48	Nambajima-watasi	3.98	0.91	4.85	0.95
	48′	Boseki-Bridge	4.01	0.92	4.88	0.96
	51	Hakurai-Bridge	3.50	0.75	4.43	0.81
	52	Ohama-Bridge	—	—	4.58	0.86
	53	Showa-Bridge	3.50	0.73	4.43	0.81

Table 3. Meximum water level and its ratio to that at thc station (1)

under construction can prevent perfectly such a class of bore, as associated with the "Jane-typhoon" under the initial water level O.P. + 1.25 m, but it is not sufficient for a bore with an initial water level O. P. + 2.00 m, and is especially very dangerous at the section where the embankment is connected steplike. In closing, it is hoped that these step-connected embankment zones will be strengthend and that more safety will be secured.

Acknowledgements

The authors wish to express their appreciation to Dr. Tojiro Ishihara, Prof. of Civil Engineering, Kyoto University and to Mr. Ichisaburo Kondo, Chief of Harbour Section, Osaka Prefecture for their helpful suggestions and encouragement. They are also greatly indebted to Messrs. Yuichi Iwagaki, Assist. Prof., Kyoto University, Atsuyuki Daido, Member of Disaster Prevention Research Institute, Tadaharu Chujo, Teacher, Fushimi High School, Masaru Hosoi, Engineer, Kyoto Prefecture, Hiroyasu Tanaka and Tadao Mats umoto, Students, Kyoto University for their kind assistance throughout the course of the present investigation.

References

1) Iwagaki, Y. "Theory of open channel flow", Proc. J.S.C.E., Vol. 39, No. 11, 1954.
2) Keulegan, G. H. "Laws of turbulent flow in open channel", Jour. of Research of N.B.S., Vol. 21, Dec., 1938.
3) Johnson, J.W. "Rectangular artificial roughness in open channels", Trans. A. G.U., 1944, Part V.
4) Hosoi, M. " On the velocity distribution and frictional resistance of the turbulent flow in open channel" (in Japanese).
5) Schlichtung, H. : "Experimentelle Untersuchungen zum Rauhigkeitsproblem", Ingenieur Archiv, Heft 1, Band 7, 1936.
6) Fergus, H. A. : "The Thames Model Investigatoin", Dock and Harbour Authority, Vol. 32, 1952.
7) Corps of Eng. ineers, U.S.Army "Study on boundary roughness in rectangular flumes", Tech. Memo., No. 2-364, 1953.

Publications of the Disaster Prevention Research Institute

The Disaster Prevention Research Institute publishes reports of the research results in the form of bulletins. Publications not out of print may be obtained free of charge upon request to the Director, Disaster Prevention Research Institute, Kyoto University, Kyoto, Japan.

Bulletins :

No. 1 On The Propagation of Flood Waves by Shoitiro Hayami, 1951.

No. 2 On the Effect of Sand Storm in Controlling the Mouth of the Kiku River by Tojiro Ishihara and Yuichi Iwagaki, 1952.

No. 3 Observation of Tidal Strain of the Earth (Part I) by Kenzo Sassa, Izuo Ozawa and Soji Yoshikawa. And Observation of Tidal Strain of the Earth by the Extensometer (Part II) by Izuo Ozawa, 1952.

No. 4 Earthquake Damages and Elastic Properties of the Ground by Ryo Tanabashi and Hatsuo Ishizaki, 1953.

No. 5 Some Studies on Beach Erosions by Shoitiro Hayami, Tojiro Ishihara and Yuichi Iwagaki, 1953.

No. 6 Study on Some Phenomena Foretelling the Occurrence of Destructive Earthquakes by Eiichi Nishimura, 1953.

No. 7 Vibration Prob ems of Skyscraper. Destructive Element of Seismic Waves for Structures by Ryo Tanabashi, Takuzi Kobori and Kiyoshi Kaneta, 1954.

No. 8 Studies on the Failure and the Settlement of Foundations by Sakuro Murayama, 1954.

No. 9 Experimental Studies on Meteorological Tsunamis Traveling up the Rivers and Canals in Osaka Citiy by Shoitiro Hayami, Katsumasa Yano, Shohei Adachi and Hideaki Kunishi, 1955.

Bulletin No. 9 Published May, 1955

昭和 30 年 4 月 30 日 印 刷
昭和 30 年 5 月 3 日 発 行

編輯兼発行者 京都大学防災研究所
印刷者 山 代 多 三 郎
京都市上京區寺之内通小川西入
印刷所 山代印刷株式会社